Journal of Volcanology and Geothermal Research 419 (2021) 107376

Contents lists available at ScienceDirect

Journal of Volcanology and Geothermal Research

journal homepage: www.elsevier.com/locate/jvolgeores

On the origin of recent seismic unrest episodes at Deception Island volcano, Antarctica

Alejandro Moreno-Vacas [a,1], Javier Almendros [a,b,*]

[a] Andalusian Institute of Geophysics, University of Granada, Spain
[b] Department of Theoretical and Cosmos Physics, University of Granada, Spain

ARTICLE INFO

Article history:
Received 7 April 2021
Received in revised form 28 July 2021
Accepted 6 August 2021
Available online 11 August 2021

Keywords:
Volcano-tectonic earthquakes
Seismic swarms
Magma intrusions
Failed eruptions
Volcano seismicity
Deception Island volcano
Antarctica

ABSTRACT

Deception Island (South Shetland Islands, Antarctica) is an active volcano characterized by a moderate level of seismic activity, dominated by long-period seismicity related to hydrothermal processes in a shallow aquifer. Nevertheless, in the last few decades the volcano has undergone at least three episodes of seismic unrest, in 1992, 1999, and 2015. During these episodes, the pattern of seismicity changed, and swarms of volcano-tectonic earthquakes with hundreds of events in time spans of a few months were detected. These episodes are interpreted as consequences of magmatic intrusions. However, the seismic series display significant differences that lead us to think that the processes initiating the series are not exactly the same in all cases. The 1999 series comprised mostly small-magnitude earthquakes, produced regularly during 1.5 months, and located at shallow depths (<4 km) within the caldera, mostly along a WSW-ENE trend that parallels the Bransfield rift. No precursory seismic activity was reported, and a few months after the series onset the seismicity was back to normal levels. The 2015 series included earthquakes with larger magnitudes, occurring during 5 months in temporal clusters separated by aseismic periods. They were located at deeper levels (<10 km) with epicenters distributed all around Deception Island, at distances up to 30 km. Additionally, distal (~35 km) VT seismicity was reported SE of Livingston Island months before the 2015 series onset, and the seismicity at Deception Island remained anomalously high during a few years. Taking into account the limited data available for the 1992 unrest, we conclude that the 1992 and 1999 series were produced by shallow, short-lived, small-volume ($\sim 4 \cdot 10^4$ m^3) intrusions that affected the shallowmost part of the volcanic edifice. On the contrary, the 2015 series was consequence of a deep, long-lasting intrusion that involved a larger volume of $\sim 5 \cdot 10^6$ m^3 (in the range of a VEI 2 eruption) and modified the stress field of the whole volcanic edifice.

1. Introduction

The Bransfield Strait is a NE-SW trending marginal basin located between the Antarctic Peninsula and the South Shetland Islands (Fig. 1). It can be divided into three subbasins: Western, Central, and Eastern (Gordon and Nowlin, 1978). The region is dominated by an extensional regime, due to the separation of the South Shetland microplate and the Antarctic plate (Catalán et al., 2013; Galindo-Zaldívar et al., 2004; Maldonado et al., 2015). The formation of the Bransfield Rift in the Late Cenozoic has been interpreted as a consequence of back-arc extension linked to the subduction of the Phoenix Plate beneath the Antarctic Plate (González-Ferrán, 1985). Several volcanic edifices are found along the rift, both subaerial and submarine.

Deception Island volcano is located at the western limit of the Central Bransfield Basin, which has a broad neovolcanic zone of seamounts and volcanic ridges (Christeson et al., 2003). It is a composite volcano with a basal diameter of 30 km, rising 1400 m from the seafloor to a maximum height of 540 m above sea level. The emerged part of the volcano forms a 15-km-wide, horseshoe-shaped island whose central part is occupied by a sea-flooded caldera (Port Foster). The volcanic evolution of Deception Island is marked by the caldera collapse, which took place between 8300 and ~3980 years BC (Antoniades et al., 2018; Oliva-Urcia et al., 2016). The pre-caldera stage was characterized by the formation of multiple coalesced shoaling seamounts and a subaerial volcanic shield (Smellie et al. 2002). The main *syn*-caldera depositional unit corresponds to pyroclastic deposits that are several tens of meters thick. The morphological features of Deception Island support a piston-like collapse model, along either ring faults or regionally induced intersecting faults, following a major eruption (Martí et al., 2013). Over 60 km^3 of magma erupted during the caldera formation event, classifying Deception Island as a medium-sized caldera, with

* Corresponding author at: Andalusian Institute of Geophysics, University of Granada, Spain.
E-mail address: vikingo@ugr.es (J. Almendros).
[1] Now at Instituto de Astrofísica de Andalucía, CSIC, Spain.

https://doi.org/10.1016/j.jvolgeores.2021.107376

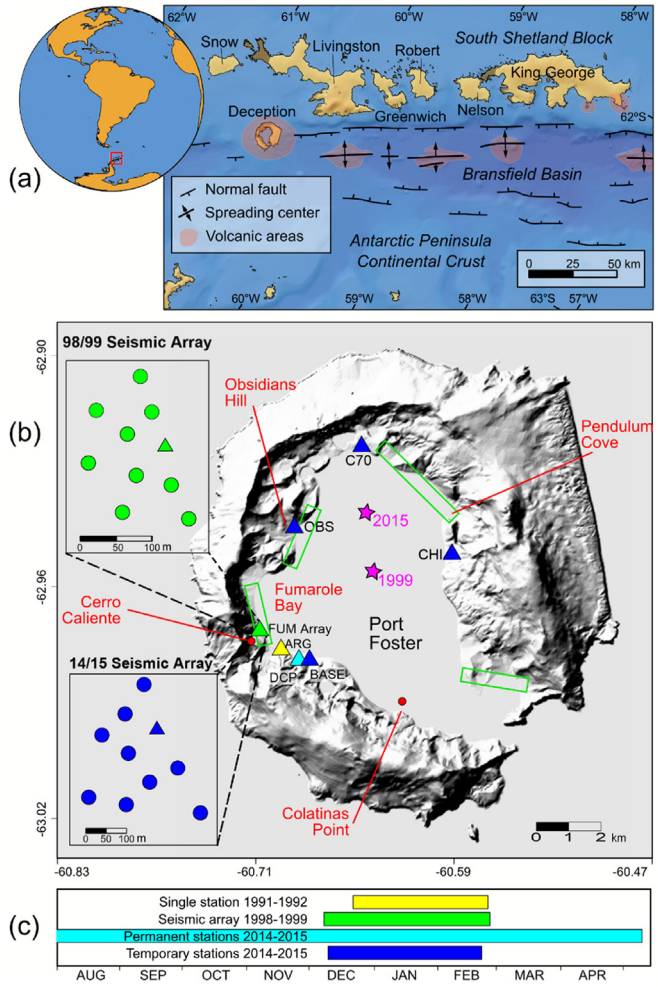

Fig. 1. (a) Map of the Bransfield Strait with the main tectonic and volcanic features of the area (modified from Jiménez-Morales et al., 2017). (b) Shaded relief map of Deception Island. Green boxes indicate fumarolic and hydrothermal areas. Magenta stars show the locations of the deformation centers of the 1999 and 2015 inflation processes. Red dots are thermometric stations. The remaining symbols represent the seismometers operating during the seismic crises: yellow for 1992 (single station ARG); green for 1999 (seismic array FUM); blue for 2015 (seismic network CHI, C70, OBS, BASE; seismic array FUM); and cyan for permanent station DCP operating since 2008. Triangles are three-component stations and circles indicate vertical-component stations. (c) Operating periods for the seismic stations recording the 1992, 1999 and 2015 seismic unrest episodes.

similar dimensions as Krakatoa or Santorini (Geyer and Martí, 2008). The post-caldera phase comprises at least 70 scattered eruptive events inside the caldera (Martí et al., 2013; Smellie et al. 2002). Recent post-caldera volcanic activity on Deception Island mostly consists of small-volume eruptions, with variable degrees of explosivity depending on the water amount that interacted with the rising magma (Baker et al., 1975; Bartolini et al., 2014; Geyer et al., 2021; Pedrazzi et al., 2014, 2018; Smellie et al. 2002). In the last two centuries, more than 20 eruptions have been reported (Bartolini et al., 2014), the most recent in the period 1967–1970 (Smellie, 2002; Pedrazzi et al. 2014).

Deception Island has an active hydrothermal system showing continuous fumarolic activity, gas emissions, and thermal anomalies. Additionally, surface deformations and a generally moderate, highly variable, level of volcanic seismicity have been reported (Almendros et al., 2018; Carmona et al., 2012; Ibáñez et al., 2003a; Ortiz et al., 1997). The seismicity includes volcano-tectonic (VT) earthquakes, produced by brittle failure of the medium within the volcanic edifice in response to changes in the stress distribution (e.g. Roman and Cashman, 2006; Zobin, 2017; Gudmundsson, 2020). In general, VT signals present an impulsive arrival, differentiated phases and a broadband spectral content. VT earthquakes are recorded before, during, and/or after a volcanic eruption, and they may also appear without eruptions (Benoit and McNutt, 1996). Deception Island produces conspicuous long-period (LP) seismicity including LP events and volcanic tremor, which are generally associated to the presence of volcanic or hydrothermal fluids that exchange elastic energy with the medium (e.g. Chouet, 2003). LP seismicity is characterized by emergent arrivals, absence of distinct phases, and narrow-band, low-frequency spectra (Ibáñez et al., 2000).

Seismic monitoring of Deception Island volcano started in the 1950s, but it was abandoned after the 1967–1970 eruptions. Sixteen years later, Spanish and Argentinean researchers began to carry out temporary surveys during austral summers, which included the acquisition of seismic data for volcano surveillance and research (Vila et al., 1992, 1995; Ortiz et al., 1992a, 1997). Since 1994, the Andalusian Institute of Geophysics, University of Granada, has carried out research projects to study the seismic activity and structure of Deception Island volcano and nearby areas (Almendros et al., 1997, 1999, 2018, 2020; Benítez et al., 2007; Carmona et al., 2010, 2012; García-Yeguas et al., 2011; Ibáñez et al., 1997, 2000, 2003a, 2003b, 2017; Jiménez-Morales et al., 2017; Luzón et al., 2011; Prudencio et al., 2013, 2015; Zandomeneghi et al., 2009). Seismic monitoring was initially limited to the austral summers (December–February), until 2008 when a permanent station was deployed at Deception Island (Carmona et al., 2014; Jiménez-Morales et al., 2017).

During the last three decades, the seismicity of Deception Island volcano displays a continuous background of LP events and tremor related to the activity of the shallow hydrothermal system (Carmona et al., 2012). This situation defines the dormant state of the volcano. However, at least in three recent occasions the seismic activity escalated (Fig. 2). These seismic crises occurred in 1992 (Ortiz et al., 1997), 1999 (Ibáñez et al., 2003b), and 2015 (Almendros et al., 2018). They were characterized by a definite increase in the number and energy of the seismic events, and most importantly, by the appearance of large numbers of VT earthquakes produced by fractures within the volcanic edifice.

In the present work, we analyze the seismicity of Deception Island volcano during the three recent seismic crises. We describe the characteristics of the seismic series, investigate the similarities and differences among them, and discuss their implications in terms of activation mechanisms.

2. Description of recent seismic unrest episodes at Deception Island volcano

2.1. The 1992 seismic series

In December 1991 a short-period, three-component seismic station was deployed near the Argentinian Base (ARG, Fig. 1, Table 1), to

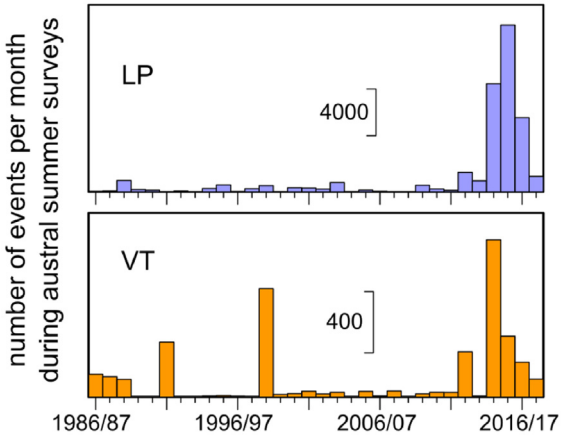

Fig. 2. Average number of VT and LP events per month recorded during the 1986–2018 monitoring surveys.

perform continuous real-time monitoring of the seismic activity during the 1991–1992 survey. Although previous seismic activity at Deception Island had been scarce (Fig. 2), 766 seismic events were recorded between 21 December 1991 and 23 February 1992 (Fig. 3a). Most of the events had magnitudes in the range 0.8 to 2, although some earthquakes were larger. In fact, four seismic events were felt, three of them with magnitudes above 3 and one reaching a maximum magnitude of 3.4.

Many earthquakes occurred in swarms lasting up to a few days. Over half of the events were followed by another event of similar characteristics within the next hour. On January 9–10, 1992 a cluster of >150 seismic events occurred very close to the ARG station, probably associated with an increase in fumarolic activity. On January 18–19 there was another seismicity increment, starting with tremor and discrete events. On February 2, 1992 there were frequent tremors and LP events. On February 25, 1992 a tremor was felt for about 2 min, although the number of seismic events was small. After a few weeks, the anomalous level of seismic activity started to decline, and by the end of February it was back to pre-1992 levels. Although the epicentral area of the recorded activity could not be determined accurately, indirect evidence showed that the source area was probably located under Fumarole Bay, just 2–3 km from the shoreline (Ortiz et al., 1997).

During the seismic series, there were also other signs of volcanic instability. For example, the area of hot soil near Fumarole Bay and Cerro Caliente appeared to be larger than in previous years. Steam emissions increased in areas with hot soils. Emissions from Cerro Caliente increased noticeably, as well as the concentration of sulfur compounds in Fumarole Bay (Ortiz et al., 1992b, 1992c, 1997).

Ortiz et al., 1997 proposed that these phenomena were a consequence of a magmatic intrusion that took place under Deception Island volcano. The intrusion of magma to shallower depths justifies the occurrence of VT seismicity, deformation, gravity variations, magnetic anomalies and changes in the fumaroles and hydrothermal system (Ortiz et al., 1997; García et al., 1997).

2.2. The 1999 seismic series

During the 1998–1999 survey, a small-aperture seismic array operated near the southern shore of Fumarole Bay (Fig. 1, Table 1). It was composed of 7 vertical-component and 3 three-component stations, with an aperture of 240 m. All instruments were short-period sensors with flat response to 1 Hz. An additional array was deployed near Obsidians Hill, although these data could not be used for source locations because they were affected by significant propagation anomalies (Saccorotti et al., 2001; Luzón et al., 2011). The Fumarole array worked between December 7, 1998, and February 25, 1999, when the Spanish base Gabriel de Castilla was closed. Due to the high level of seismicity at the end of the field survey, a vertical-component seismic station was left near the Spanish base, which operated for a few more weeks.

During December 1998 only 8 VT events were recorded, a rate similar to the average of a few tens of events per season obtained in previous years (Ibáñez et al., 2000). However, starting on January 4, 1999, there was a sharp increase in the number of VT earthquakes (Fig. 3a). Approximately 1200 VT earthquakes were reported in ~1.5 months, with delays between the S and P phase arrivals (S–P times) up to 4 s and magnitudes in the range from −0.8 to 3.4. Event rates of tens of earthquakes per day were often recorded, reaching a maximum of 80 VT events per day on January 20. The staff working on the island felt two of these VT earthquakes, on January 11 and 20. At the end of the field survey, the seismic activity was still high, often with more than 50 VTs per day. The station left at the base recorded a high level of seismicity also through March and early April (Ibáñez et al., 2003b), without any indication of the termination of the series. Nevertheless, in the next survey (November 1999) the level of seismicity was back to normal (Carmona et al., 2012).

Among the VT earthquakes recorded at the Fumarole array, 863 events were located using array methods (Del Pezzo et al., 1997; Almendros et al., 1999). Most earthquakes had apparent slownesses around 0.3 s/km, and concentrated around two main back-azimuths of 45°N and 80°N, both in the NE quadrant toward Port Foster. Hypocenter locations were determined from the apparent slownesses, back-azimuths, and S–P times in a velocity model adequate for Deception Island (Ibáñez et al., 2000, 2003a). The results indicate that VT seismicity was shallow, with depths of 1–4 km, and confined mostly to the inner bay of Deception Island. Hypocenters cluster near the array site (Fig. 3b), although they also extend in the two directions mentioned above (Ibáñez et al., 2003b). These directions coincide with fracture systems described in the northern sector of Deception Island (Martí et al., 1996, 2013; Paredes et al., 2006; Maestro et al., 2007).

Swarms of LP seismicity with durations of a few days were also produced. About 1800 LP events were recorded during the series, reaching a peak activity of 150 events per day. However, this LP activity was considered normal for Deception Island. Additionally, array results for 350

Table 1
Summary of significant parameters of the seismic series: instruments and operation periods; onset and duration of the seismic series; number of VTs reported; magnitude range, epicentral locations, and depth range; deformation and other observations.

	1992	1999	2015	
			proximal	distal
Instruments	Single station ARG	Seismic array FUM	Seismic network + array FUM	Permanent stations DCP, LVN
Recording period	21 Dec 1991–24 Feb 1992	07 Dec 1998–22 Feb 1999	1 Dec 2014–24 Feb 2015	up to 9 May 2015
Series onset	<21 Dec 1992	4 Jan 1999	9 Dec 2014	15 Aug 2014
Series duration	>2 months	>1.5 months	>5 months	>8 months
Number of VTs	766*	863	703	8888
Magnitude range	Most 0.8–2; max 3.4 (4 felt)	−0.8 to 3.3 (2 felt)	−1.1 to 3.3	−0.4 to 4.6
VTs M > 1	–	138	549	5293
VTs M > 1 located	–	138	255	390
Epicentral location	Fumarole Bay?	Within Port Foster	Scattered around Deception	SE of Livingston
Depth range	Shallow?	0–10 km (most 0–4 km)	0–25 km (most 0–10 km)	0–25 km (most 0–10 km)
Deformation	Local uplift?	Inflation (Mogi depth 3.8 km)	Inflation (Mogi depth 6.1 km)	–
Other observations	Cerro Caliente emissions, gravity changes	Sulfur deposits at Fumarole Bay	Precursory seismicity DCP, temperature in Colatinas, Cerro Caliente	–
Relevant reference	Ortiz et al., 1997	Ibáñez et al., 2003b	Almendros et al., 2018	

* Total number of volcanic events (VT + LP).

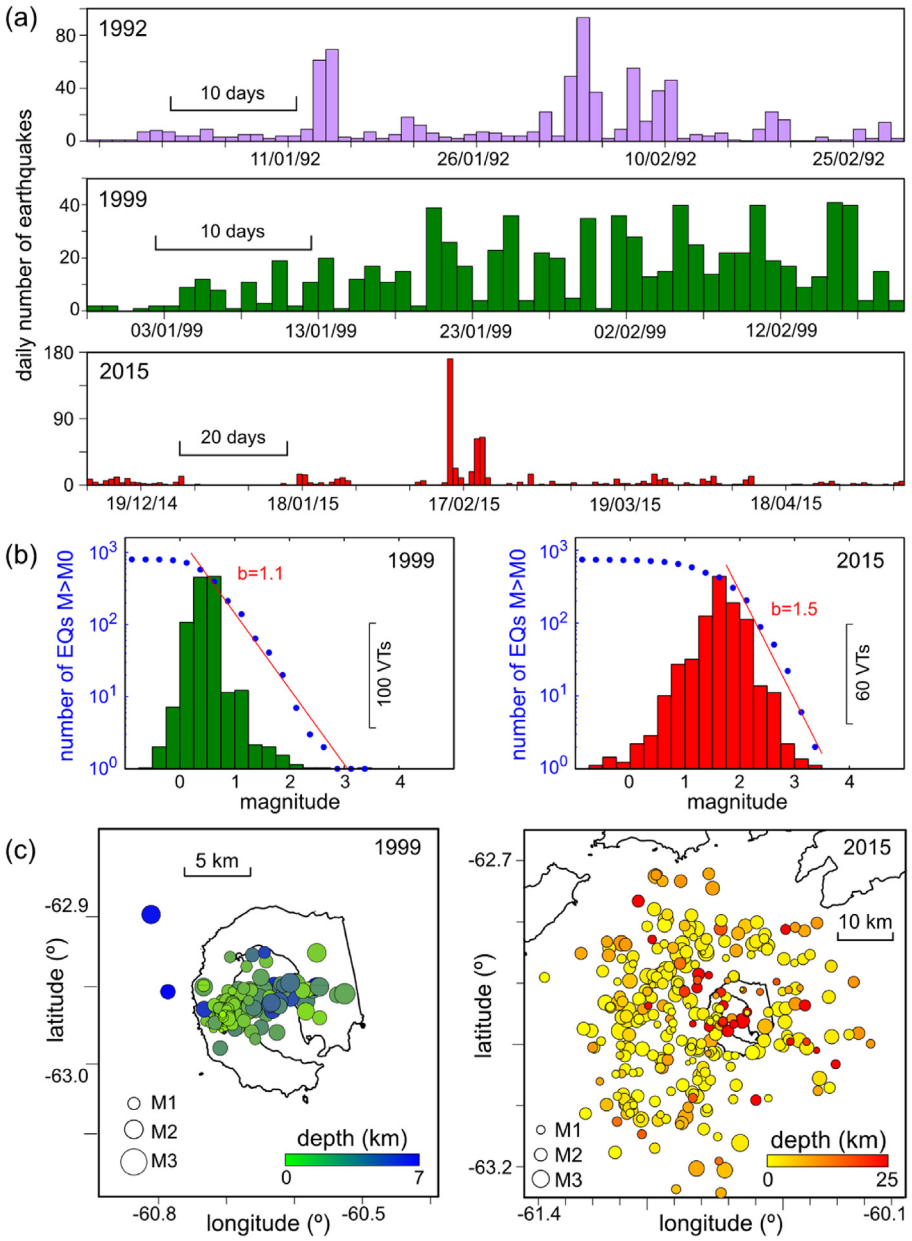

Fig. 3. Summary of relevant results for the 1992, 1999, and 2015 seismic series, as reported by Ortiz et al., 1997, Ibáñez et al., 2003b, and Almendros et al., 2018. (a) Daily number of earthquakes from December 26, 1991 to February 28, 1992 (top, violet); December 29, 1998 to February 19, 1999 (middle, green); and December 9, 2014 to May 9, 2015 (bottom, red). For 1999 and 2015 the numbers represent VT earthquakes only. (b) Frequency-magnitude distribution and estimate of the b parameter of the Gutenberg-Richter law for the 1999 and 2015 series. (c) Epicentral maps displaying the source locations, magnitudes (size), and depths (colour) of VT earthquakes in the 1999 (green-blue) and 2015 (yellow-red) series.

LP and tremor events yielded back-azimuths around 270°N and apparent slownesses of ~0.8 s/km (Ibáñez et al., 2003b). Therefore, there was no spatial relationship between the LP and VT seismicity sources.

The 1999 seismic activity was accompanied by changes in the fumarolic gases. Different studies analyzed their compositions before (1993–1998) and after (2000, 2002, 2003–2004) the seismic crisis (Caselli et al., 2004, 2007). Initially, the fumaroles located on Fumarole Bay had a strong hydrothermal character, being systems at low pressures and dominated by water vapor (Casadevall and Greenland, 1981). After the seismic crisis, there was a noticeable increase in the concentration of sulfur dioxide. Additionally, the fumaroles tended to homogenize their compositions, which had been previously quite distinct. These changes were interpreted as consequences of an enhanced gas flux from depth that increased the amount of magmatic species and reduced the interactions with the shallow aquifer (Caselli et al., 2004, 2007).

As for the 1992 seismic series, the model that best explains the origin of the 1999 seismic series is a magmatic intrusion (Ibáñez et al., 2003b) that stalled before reaching the surface of Deception Island.

2.3. The 2015 seismic series

During the 2014–2015 survey, five short-period, three-component seismic stations were located around Port Foster (Fig. 1, Table 1). Surrounding station FUM, on the southern shore of Fumarole Bay, nine vertical-component seismometers were deployed as a small-aperture (~340 m) seismic array with similar location and configuration than the 1999 array. Additionally, since 2008 three permanent, broadband

seismic stations were maintained in the area, one of them (DCP) at Deception Island and another one (LVN) at the nearby Livingston Island (Carmona et al., 2014; Jiménez-Morales et al., 2017). Continuous data records are available from December 2014 to February 2015 for the short period network and seismic array; and up to April/May 2015 for the permanent stations (Almendros et al., 2018).

VT earthquakes occurred sporadically at Deception Island volcano in early December 2014. Later they became more frequent and started to group in clusters (Fig. 3a), with S–P delays in the range 1–6 s. The two clusters on February 14–15 and 18–21 were especially significant in terms of earthquake numbers and energy. Some earthquakes in the late February clusters had large magnitudes up to 3.3. The seismic activity continued through March and April, displaying lower S–P delays and magnitudes, and it was still relevant when the DCP station stopped working in May 2015 (Almendros et al., 2018).

Source distances based on S–P delays were estimated for 773 earthquakes recorded by the temporary network and DCP station. Source locations based on phase arrival times to the stations of the temporary network were obtained for 298 earthquakes between December and February (Fig. 3b). The early clusters were located SW of Deception Island, although in February epicentral locations surrounded the volcano in all directions. Depths were mostly limited to the first 10 km of the crust.

LP events displayed a sharp increase compared with previous surveys (Fig. 2). The total number of LP events recorded during the survey increased one order of magnitude compared to previous surveys. This reveals a higher activity in the hydrothermal system, which had been altered by the mechanism producing the series.

Other signs of increasing instability were detected before the 2015 seismic crisis, thanks to the long-term monitoring of the volcano. For example, significant variations in the temperature trends of the Port Foster seawater and the Cerro Caliente hot spot were observed in 2012 (Berrocoso et al., 2018). Similarly, the number of long-duration volcanic tremors increased between 2012 and 2015 (Jiménez-Morales et al., 2017).

Additionally, three months before the onset of the 2015 crisis at Deception Island, a seismic swarm started near Livingston Island (Almendros et al., 2015, 2018). The series began in late August 2014, and lasted for ~8 months, overlapping the Deception Island VT series. About 9000 earthquakes were detected (Fig. 4), most of them with S–P delays at station LVN in the range 2.9–3.5 s. The epicenters clustered in a region southeast of Livingston, close to Humpback seamount, at about 35 km NE from Deception Island. Earthquake magnitudes ranged up to 4.6, with a total cumulative seismic moment of $7.8 \cdot 10^{16}$ N·m, equivalent to a magnitude 5.2 earthquake.

3. Comparison among seismic series

The three recent seismic series reported at Deception Island are thought to be originated by the same mechanism, i.e. a magmatic intrusion under the volcano that alters the stress state and triggers the occurrence of VT seismicity in brittle regions of the volcanic edifice. In the following, we compare these series in detail, and describe the similarities and differences among them. More effort will be put in the 1999 and 2015 series, for which complete earthquake catalogs are available. In the case of the 1992 series, we only have the information and figures published in Ortiz et al., 1997.

First, we note that the three series have been recorded with different instruments: a single station for the 1992 series; a small-aperture seismic array for the 1999 series; and a local seismic network for the 2015 series. This fact imposes some limitations in our ability to compare the results. For example, in the 1999 catalog we find many earthquakes with small magnitudes (Fig. 3b). They could be adequately detected and located because: (1) they occurred in Fumarole Bay, close to the seismic array; similar small-magnitude earthquakes in other areas of the island would not be detected at all; and (2) they were located using array techniques that exploit the signal coherence to extract information about the seismic wavefield, even at low signal to noise ratios. Ibáñez et al., 2003b demonstrated that the concentration of small-magnitude earthquakes around the array site in 1999 was an apparent effect due to their low magnitudes. On the contrary, the distribution of earthquakes with M > 1 was homogeneous across Deception Island, and encompassed basically the whole of Port Foster. These

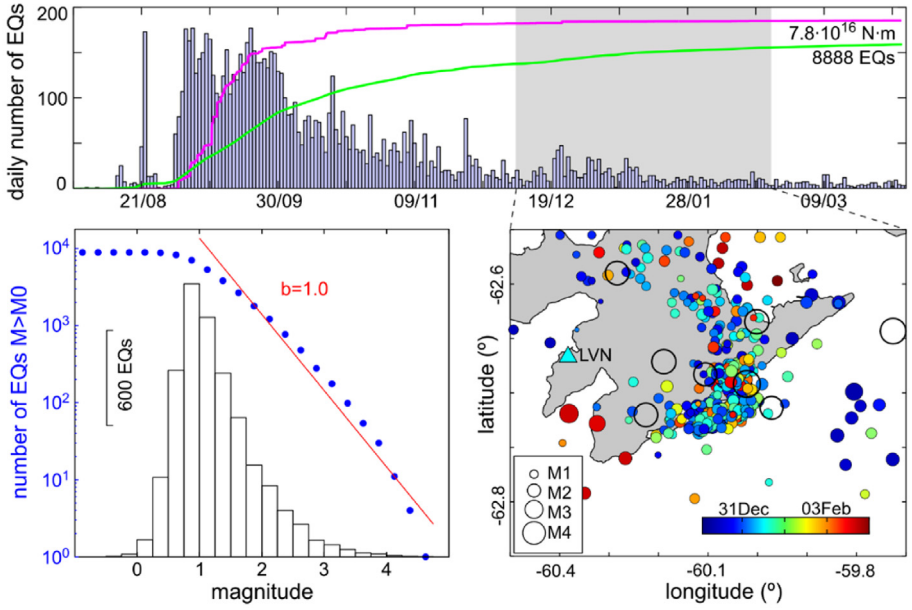

Fig. 4. Summary of results for the 2014–2015 Livingston series, as reported by Almendros et al., 2018. (top) Daily number of earthquakes from August 2014 to April 2015. The green and magenta lines are the cumulative number of earthquakes and cumulative seismic moment, respectively. The gray box indicates the period of operation of a temporary seismic network that allowed for source locations. (bottom left) Frequency-magnitude distribution and estimate of the b parameter of the Gutenberg-Richter law. (bottom right) Epicentral map displaying the earthquake locations, magnitudes (size), and origin times (colour). Open circles correspond to the largest earthquakes of the series, occurring in September–October, as reported by global catalogs (ISC 2021). The cyan triangle marks the location of the permanent station LVN.

small-magnitude earthquakes cannot be located with an island-wide seismic network, as the one deployed in 2015. Even if they were close enough to one station to be detected, they would not be recorded at more distant stations, precluding our ability to perform a location based on phase arrival times.

In order to avoid these effects and make the series comparable, we select earthquakes with magnitudes larger than 1 (Table 1). With this constraint, the total number of VT earthquakes in the 1999 catalog reduces drastically to 138. The 2015 catalog is less affected, given that the reported earthquakes are generally larger, and contains 549 earthquakes. This means that there were four times more VT earthquakes during the 2015 series, which seems to be a large difference; however, we have to consider the lengths of the recording periods. The 1999 series started on January 4, 1999, and the data records span until February 20 (48 days). The onset of the 2015 crisis is not as clear. We consider that it started on December 9, 2014, when the first VT cluster took place. In this case, the data cover until May 9, 2015 (151 days). Taking into account the swarm durations, the average earthquake production rates for the 1999 and 2015 series are about 2.9 and 3.6 VT earthquakes per day, respectively. These estimates indicate that, although the 2015 series was slightly more active than the 1999 series, both of them yielded comparable numbers of events (around a hundred earthquakes per month).

3.1. Temporal distribution

The temporal distributions of the seismic series at Deception Island do not follow a typical mainshock-aftershock sequence. For a tectonic series, the number of aftershocks often decreases quickly with time (Omori law). In the Deception series there are no mainshocks and the VT earthquakes occur during long time periods of several months, at rates that are highly variable but do not generally show a constant decay with time. This observation corroborates the hypothesis that the origins of the seismic series are related to continuous processes driven by the dynamics of Deception Island volcano.

Although the similarity of the earthquake production rates during the 1999 and 2015 series suggest a common behavior, in reality the temporal occurrence of VT earthquakes followed completely different patterns (Fig. 5). In 1999 VT events occurred regularly, with similar numbers of VTs recorded every day, up to a maximum of 10 earthquakes per day, and very few days without any seismic activity. Accordingly, the cumulative number of earthquakes shows a continuously increasing trend, with an initial slope of 1.1 VTs/day in early January, 1.5 VTs/day in mid-January, and 3.9 VTs/day later on (Table 2). Therefore, the 1999 crisis was characterized by a distributed generation of VT events all over the recording period, with earthquakes occurring every day. On the contrary, in 2015 the series behavior was more irregular. Two periods concentrated most of the VT earthquakes, namely February 14–15 and February 19–21 (Fig. 5), with production rates up to 208 and 49 VTs/day, respectively (Table 2). Apart from these and other peaks of activity, there were also long periods when virtually no earthquakes were produced. The cumulative number of earthquakes reflects this irregular behavior, with sudden jumps corresponding to the peaks of earthquake activity. Thus, the 2015 crisis was discontinuous and released seismic energy in a few surges of several tens of VT events per day, while most days were characterized by very few VTs, if any.

The different temporal behaviors are also evident from the analysis of the repose times (Fig. 6). In the 2015 series there were long gaps with no seismic activity, and most earthquakes occurred shortly after another earthquake, in dense temporal clusters. In fact, 69% of the VT earthquakes were followed by another earthquake within one hour. In the 1999 series the repose times were more heterogeneous, confirming again the continuous distribution of earthquakes along the recording period. In this case, only 27% of the events were followed by another event within one hour, and about 40% of the events were not followed by another earthquake for more than 5 h.

In 1992, the temporal distribution of earthquakes (Fig. 3a) was discontinuous and episodic, displaying days with up to 100 seismic events and days with very little seismic activity. The distribution of repose times between seismic events (Fig. 6) indicates that 72% of the seismic events were followed by another event within one hour. This behavior is similar to the 2015 series, and contrasts with the more regular temporal pattern of the 1999 series. However, we do not know how many of the seismic events reported were VT earthquakes. The peaks of activity on January 9–10 and February 1–4 were dominantly composed of hundreds of LP events (Ortiz et al., 1997). Therefore, we do not know if the

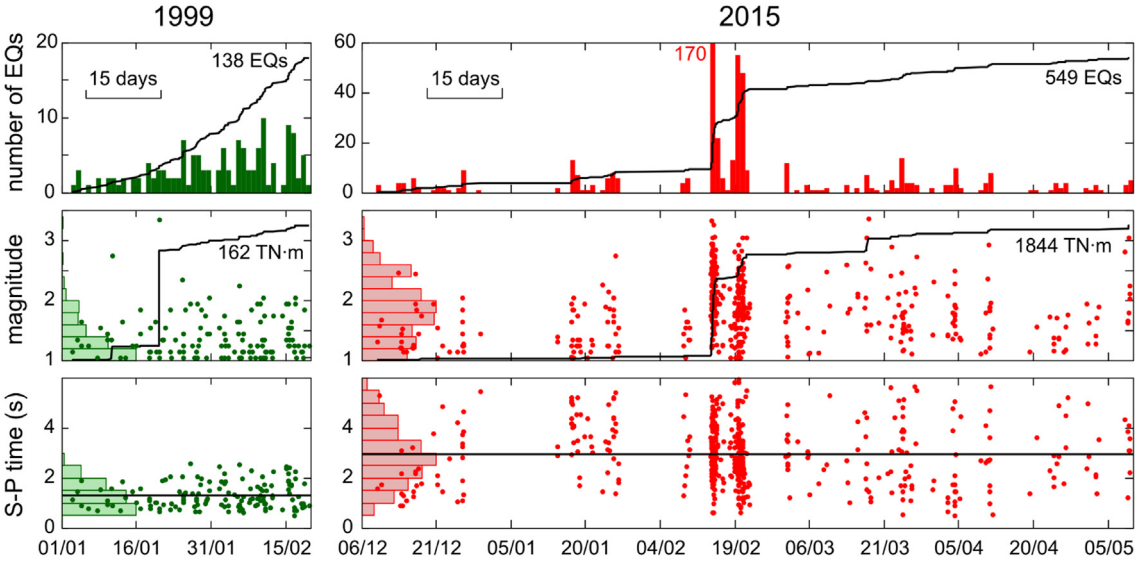

Fig. 5. Comparison between different characteristics of the 1999 (green, left) and 2015 (red, right) seismic series, for VT earthquakes with magnitudes above 1. The horizontal axis represents time, displayed at the same scale in all plots. [top] Temporal occurrence of earthquakes. Vertical bars represent the daily number of VT earthquakes. The continuous line indicates the cumulative number of events throughout the series. The numbers at the end of these lines are the total number of earthquakes. [middle] Magnitude distribution of the seismic series. Dots represent the VT earthquake magnitudes. The continuous line is the cumulative seismic moment. The numbers at the end of these lines represent the total seismic moment released. The histograms on the left side of each plot illustrate the magnitude distributions. [bottom] S–P delay times of the VT earthquakes (dots). The histograms on the left side of each plot represent the S–P delay distributions.

Table 2
Average daily earthquake production and seismic moment release rates during selected periods in the 1999 and 2015 seismic series.

	time period	Earthquake production rate (EQs/day)	Seismic moment rate (10^{12}N·m/day)
1999 series	03/01/1999–11/01/1999	1.05	0.14
	11/01/1999–20/01/1999	1.54	0.25
	20/01/1999–20/02/1999	3.89	1.02
	average 1999	**2.92**	**3.40**
2015 series	09/12/2014–29/12/2014	1.82	1.00
	14/01/2015–26/01/2015	3.45	2.26
	08/02/2015–09/02/2015	6.17	1.49
	14/02/2015–15/02/2015	208	1150
	15/02/2015–19/02/2015	6.69	7.54
	19/02/2015–21/02/2015	48.6	146
	01/03/2015–17/03/2015	1.40	3.15
	17/03/2015–11/04/2015	2.66	4.11
	11/04/2015–09/05/2015	1.22	2.62
	average 2015	**3.63**	**12.2**

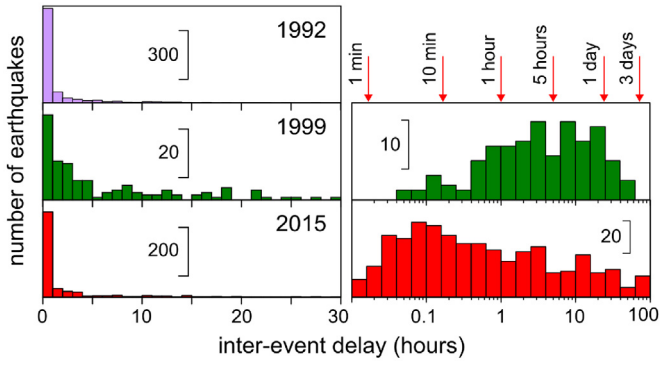

Fig. 6. Histograms of the delay time between consecutive events for the 1992 (top, violet), 1999 (middle, green) and 2015 (bottom, red) series. The data are shown with linear bins (left) and logarithmic bins (right). For the 1992, we show only the linear version due to the lack of quantitative data.

VT distribution is in fact episodic, or rather we are just observing an effect due to the superposition of VT and LP distributions.

3.2. VT magnitudes

Earthquake magnitudes have been estimated using different methods. In 1999, Ibáñez et al., 2003b calculated the moment magnitude from the amplitude of the low-frequency spectrum. For the 2015 series, Almendros et al., 2018 applied a coda duration scale adjusted for Deception Island (Havskov et al., 2003). In spite of this difference, these magnitudes can still be used as a first approximation to compare the seismic energy released in both series.

Fig. 5 shows the magnitude distributions for VT events recorded during the 1999 and 2015 series. The maximum magnitudes reported for these series are both 3.3. However, if we analyze the magnitude distributions we find significant differences between them. In the 2015 series, earthquakes had generally larger magnitudes. For example, in the 1999 series about 75% of the earthquakes had magnitudes between 1 and 1.5. In the 2015 series, only 25% of the earthquakes had magnitudes in that range. Accordingly, the average magnitudes are 1.3 in 1999 and 1.9 in 2015.

The Gutenberg-Richter law represents the partition between small and large earthquakes. Tectonic series generally comply with the Gutenberg-Richter law with a *b* parameter near 1, while for volcanic series we find more variability, with *b* ranging from 1 to 3 (McNutt, 2005; Roberts et al., 2015). Fig. 3b shows that the 1999 catalog is complete for $M > 0.5$ and we can estimate a *b* value of 1.0–1.1. For the 2015 series, the completeness magnitude is higher, and the calculations are less reliable. Our estimates are in the range 1.0–1.6, perhaps indicating a faster decay in the number of large earthquakes.

The total seismic moment released during the 1999 series was $1.6 \cdot 10^{14}$ N·m, which represents an average release of $3.4 \cdot 10^{12}$ N·m/day. The total moment of the 2015 VT series was $1.8 \cdot 10^{15}$ N·m, which yields a rate of $12.2 \cdot 10^{12}$ N·m/day. Therefore, the average seismic moment release rate during the 2015 series is about 4 times the 1999 value. In terms of equivalent magnitudes, the total seismic moment in 1999 is equivalent to a magnitude 3.5 earthquake, while the moment released in 2015 is equivalent to a magnitude 4.2 earthquake.

The cumulative seismic moment is shown in Fig. 5. As for the cumulative number of earthquakes, we observe clear differences in the temporal evolution of the cumulative moment for the two seismic series. In 1999 we observe small seismic moment rates, except for the jumps produced by the two largest earthquakes on January 11 and 20. Moment rates were $1.4 \cdot 10^{11}$ N·m/day in early January, $2.5 \cdot 10^{11}$ N·m/day in mid-January, and $1.0 \cdot 10^{12}$ N·m/day for the remaining period (Table 2). On the other hand, in the 2015 crisis the moment rates were highly variable. There were periods with no seismicity, and thus the cumulative seismic moment is flat. However, several periods had significant moment release rates reaching $1.1 \cdot 10^{15}$ N·m/day on February 14–15, $1.5 \cdot 10^{14}$ N·m/day on February 19–21, $7.5 \cdot 10^{12}$ N·m/day on February 15–19, and $4.1 \cdot 10^{12}$ N·m/day from March 17 to April 11 (Table 2). These values are larger than the 1999 rates, and much more variable. While in 1999 moment rates span one order of magnitude, in 2015 the variations reach three orders of magnitude (without considering the frequent aseismic periods).

These results demonstrate that although the maximum magnitudes were comparable, the 2015 crisis was more energetic than the 1999 series. Additionally, the energy release was continuous during the 1999 series, and quite irregular during the 2015 series.

For both series, at the end of the recording periods there were no evidences suggesting an imminent ending of the seismic series. Seismic moment rates were still high, with values of $1.0 \cdot 10^{12}$ N·m/day in February 1999 and $2.6 \cdot 10^{12}$ N·m/day in May 2015. Similarly, the cumulative numbers of events still showed growing trends of 3.9 and 1.2 events/day, respectively. Therefore, the two series were not over yet when the seismic stations were removed, and the total series durations are unknown. For the 1999 series, the VT activity was back to normal by the start of the next survey (December 1999). For the 2015 series, the VT activity was still high during the next few surveys (Fig. 2).

3.3. VT locations

The spatial distributions of VT sources were extremely different in the 1999 and 2015 series. A first hint comes from the ranges of S–P delays (Fig. 5) that are related to the distance to the earthquake source. In 1999 most VT earthquakes had S–*P* values between 0.5 and 2.5 s, with an average of 1.3 s. On the contrary, in 2015 the S–P delays ranged between 1 and 5.5 s, with a higher average of 3.0 s. This difference suggests that, in general, the 2015 earthquakes were located either deeper or farther from Deception Island than the 1999 earthquakes.

Fig. 7 compares the epicentral maps of the 1999 and 2015 series, for earthquakes with $M > 1$. In 1999 all events clustered within Port Foster at distances smaller than 10 km from the center of the caldera. The epicenters follow an alignment at 80°N from the array site across Port Foster. Earthquake depths were generally limited to the first 4 km of the crust, although some events had depths down to 10 km. This distribution suggests the activation of a well-defined fault system across the caldera, coinciding with the direction of the Bransfield rift, which has been described by many authors (Martí et al., 1996, 2013; Paredes et al., 2006; Maestro et al., 2007). Some of the VT earthquakes had similar waveforms, which suggests the repeated activation of the same sections

of the faults (Ibáñez et al., 2003b). Using a cluster analysis, 225 VT earthquakes were classified into 48 different families (Carmona et al., 2010). Additional analyses based on precise relocations using array techniques (Almendros et al., 2004) allowed for the precise location of 14 clusters of VT earthquakes, and showed that the structures responsible for the VT earthquakes were sub-vertical faults oriented mostly NW-SE (Carmona et al., 2010).

In 2015 the earthquake distribution was substantially different. Epicenter locations encompassed Deception Island at distances ranging up to 30 km (Fig. 7). No clear trends were observed in the epicentral distribution, apart from the fact that the earthquakes tended to occur mainly westward of Deception Island. Earthquake depths were larger than in 1999, with most VT earthquakes occurring in the first 10 km of the crust and maximum depths of ~30 km. This scattered pattern contrasts with the tight linear distribution of the 1999 epicenters, indicating that the seismicity was not generated by a single seismogenic structure as in 1999. And quite accordingly, in the 2015 series there were no evidences of similarities in the VT waveforms. The 2015 hypocenters are widespread throughout the volcanic edifice. Therefore, the series corresponded to a generalized activation of multiple faults across the volcanic edifice and especially beneath its western flank.

Barclay et al., 2009 analyzed the bathymetry around Deception Island volcano. They report several sets of fault scarps, most of which are oriented in ENE-WSW direction (coincident with the rift). The densest populations are located W-SW and E-NE of Deception, again coinciding with the inferred position of the Bransfield rift. South of Deception Island they describe faults with different directions that could be related to the radial stress generated by the volcano. These faults could promote the propagation of stress, and produce distal earthquakes both NE of Deception (near Humpback volcano) and SW (near Sail Rock), where some clusters of earthquakes appeared in December 2014 and January 2015. Nevertheless, a significant part of the seismicity comes from the NW of Deception Island. In this region, we are near the South Shetland shelf, and no evidences of faults can be found in the bathymetry.

The differences between the spatial distributions of earthquakes in 1999 and 2015 are significant even when we consider the uncertainties associated to the source location process and the diverse location methods (waveform cross-correlation in a dense seismic array in 1999 versus phase arrival times in a distributed network in 2015). Location uncertainties are large, mostly due to the limitations of the instrument deployment. For example, the seismic network configuration is limited by the extent of the island. It is perfectly suited for the location of earthquakes within Deception Island, but in 2015 many earthquakes occurred well outside the network. Almendros et al., 2018 were able to achieve estimates of epicentral locations and depths of the VT events, although the uncertainties associated with the source locations are large. We estimate that these uncertainties can be of ~1 km in the center of the network, and ~ 10 km at distances of 20 km from the island. Similarly, in the 1999 series Ibáñez et al., 2003b reported that location errors were around 1 km for earthquakes located in the center of Port Foster. In any case, even with these uncertainties, the spatial distributions of Fig. 7 are substantially different.

Although earthquake locations could not be accurately determined for the 1992 series, Ortiz et al., 1997 used indirect evidence to suggest that the source of the seismic activity was shallow, and was located near the ARG station (Fig. 1) at distances of just a few kilometers. This range of distance seems to be consistent with the hypocenter pattern obtained for the 1999 series. In this sense, it is noteworthy to point out that during the 1992 series four earthquakes with magnitudes between 2.7 and 3.4 were felt by the scientists and technicians working in the area (Ortiz et al., 1997). In 1999, the two largest earthquakes with magnitudes 2.7 and 3.3 were also felt. In 2015, there were 33 earthquakes with magnitudes above 2.7, but despite the similar magnitudes, none of them were felt by the scientists and technicians in the Gabriel de Castilla Base (Almendros et al., 2018). Thus, we image the 1992 hypocenters as being close enough to the Argentinian Base for a M3 earthquake to be felt. Such spatial pattern is more similar to the tight source locations of 1999 than to the widespread distribution of 2015.

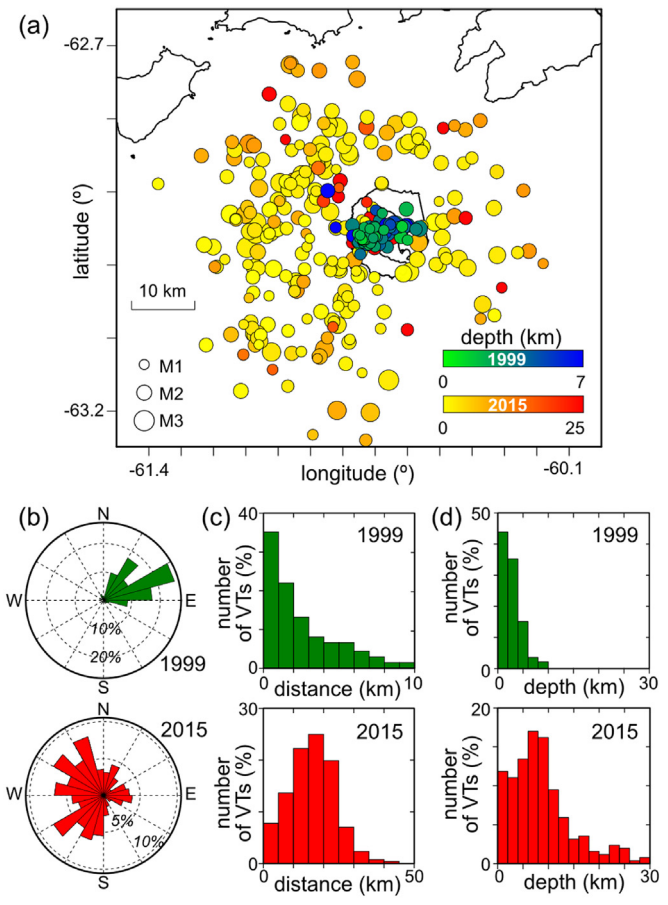

Fig. 7. (a) Epicentral map of VT earthquakes of the 1999 and 2015 seismic series, for magnitudes greater than 1. The symbol sizes represent the earthquake magnitudes, and the colors indicate the source depths. (b) Back-azimuth distributions of the 1999 and 2015 series for magnitudes greater than 1, as seen from the FUM array site (Fig. 1). The colored bars indicate the percentage of earthquakes in a given direction. (c) Histogram of the epicentral distances of the 1999 and 2015 series for magnitudes greater than 1. (d) Same as (c) for the depth distributions.

3.4. Other observations

The seismicity of Deception Island volcano is dominated by the conspicuous presence of LP events and tremor. Although the levels of LP seismicity are variable, they have generally increased during the seismic series. This phenomenon is especially evident in the 2015 series, when the number of LP events increased one order of magnitude in comparison to previous surveys (Fig. 2). However, the characteristics of the LP seismicity remained stable, indicating that LP seismicity was not apparently linked to the VT source. The waveforms, frequency contents, source areas and mechanisms were the same before, during, and after the VT series. Therefore, LP seismicity during the series was still related to instabtilities in the shallow hydrothermal system, and not a direct consequence of magma motions. The observed increase in LP seismicity was interpreted as an indirect effect of the intrusion process, due to increased flux of gases and/or heat through the hydrothermal system (Nakano and Kumagai, 2005; Cusano et al., 2008; Jolly et al., 2017).

The long-term variations of seismicity before the seismic series could not be addressed until the permanent seismic station DCP was installed in 2008. Thanks to this dataset, we know that there were several phenomena preceding the 2015 series, such as the increase in the

number of long-duration volcanic tremors after 2012 (Jiménez-Morales et al., 2017), the occurrence of a seismic series SE of Livingston Island in 2014 (Almendros et al., 2018), and a continuous increase in VT earthquake activity (Jiménez-Morales et al., 2021, submitted). For the 1992 and 1999 series, the datasets are limited to the survey durations, and no information about previous events is available. Therefore, we cannot compare the long-term behavior of the seismicity before the seismic series.

Apart from the seismological observations, the seismic series were accompanied by variations in other parameters. One important parameter at Deception Island volcano is deformation, which has been periodically monitored since 1991. Rosado et al., 2019 analyze the time series of GPS observations between 1991 and 2018. They propose that the periods of high seismic activity at Deception Island volcano are preceded by inflation phases, as indicated by the extension and uplift measured in the geodetic network, and followed by deflation phases. For the 1992 series there is a gap in the GPS data, but the comparison between the displacements obtained in the 1991–1992 and 1995–1996 surveys indicate that at some point an inflation process took place, with an estimated radial deformation of 2.1 cm/year. The deformation observed on the island in 1998–1999 shows an inflation and uplift process, with average radial deformation of 5.2 cm/year, and vertical uplift of 5.5 cm/year. These are the fastest deformation rates reported for Deception Island until the 2019–2020 survey (M. Berrocoso, personal communication). Similarly, before the 2015 series there was another inflation process, with deformation rates of 1.9 cm/year between 2013 and 2015. In all cases, the inflation processes could be roughly represented by a Mogi source located beneath Port Foster, with a volume change near 0.01 km^3, similar for all three processes. Estimates of the Mogi source depth yielded values of 6.8 km in 1992, 3.8 km in 1999, and 6.1 km in 2015 (Rosado et al., 2019).

Variations in other parameters have been occasionally reported. For example, Ortiz et al., 1997 mentions microgravity changes in the Argentinian Base area during the 1992 series. Caselli et al., 2004 describe changes in fumarole temperatures and gas compositions during the 1999 series, and the closing of the inner lake near the Argentinian Base, likely due to an uplift process. Berrocoso et al., 2018 report changes in seawater and hot soils temperatures three years before the 2015 series. However, these continuous temperature observations were not available before 2008, and therefore we cannot compare their behavior during the three seismic series.

4. Magmatic intrusions at Deception Island

The 1992, 1999, and 2015 series described above share some common characteristics. They lasted for a few months; produced similar numbers of VT earthquakes (about a hundred $M > 1$ earthquakes per month); and reached maximum magnitudes of 3.3–3.4. During the series, the levels of LP events and tremor generally increased, although their characteristics suggest that they were not linked to the VT source (Ibáñez et al., 2003b). The series were preceded by inflation and followed by deflation, with the centers of the deformation located beneath the Deception Island caldera (Rosado et al., 2019). Other observations have been reported as well, such as temperature changes and variations in gas compositions.

Several models could explain the origin of these seismic series. For example, they could be produced by tectonic stresses related to the extension of the Bransfield rift. In this sense, the earthquakes would be the response of local faults to the variations in regional tectonic stress (Roman and Cashman, 2006; Cembrano and Lara, 2009; Jay et al., 2015). Another mechanism is related to the dynamics of the shallow hydrothermal system. The circulation of fluids and hydrothermal alteration of the host rock may induce swarms of shallow earthquakes (e.g. Heinicke et al., 2009; Mesimeri et al., 2021). However, the observation of island-wide inflation, temperature anomalies, changes in gas compositions, and microgravity variations, lead us to think that the volcano dynamics must play an active role in the generation of the seismic series.

Therefore, we propose that the seismic series were consequences of shallow magma intrusions that altered the equilibrium of the Deception Island volcanic system but did not produce eruptions (Ortiz et al., 1997; Ibáñez et al., 2003b; Almendros et al., 2018). The plumbing system of Deception Island volcano is imaged as a combination of sills, dykes and conduits at different depths. The intrusion of magma into one of these accumulation zones induces alterations in the stress field of the volcanic edifice. Consequently, the brittle regions display an increased rate of VT earthquakes, producing the seismic series. The intrusion is also responsible for the increase in internal pressure that produces the inflation/deflation cycles. It also explains the changes in gas emissions and temperatures, related to the enhanced gas and heat supply from a fresh magma batch. Although there is magma ascent, no eruption occurs. The intrusion loses energy during its ascent and stalls at some depth. The process seems to have a duration of a few months, after which the system returns to a stable state.

Similar series of events are common to active volcanoes around the world. Examples are the 1966–1967 seismic swarm at Soufriere Hills volcano, Montserrat (Shepherd et al., 1971); the 1996 swarm of VT earthquakes beneath Akutan Island, Alaska (Lu et al., 2000); the 1996–1997 VT swarm at Iliamna Volcano, Alaska (Roman and Power, 2011); the 1998 seismic series at Iwate volcano, Japan (Nishimura and Ueki, 2011); the 2004–2005 seismic activity at Teide volcano, Canary Islands (Almendros et al., 2007; Domínguez-Cerdeña et al., 2011); the major seismic swarm recorded near Paricutin volcano, Mexico, in 2006 (Gardine et al., 2011); the 2009 seismic activity in the basaltic field of Harrat Lunayyir, Saudi Arabia (Koulakov et al., 2015); or the volcanic unrest at La Soufriere in Guadaloupe, French Indies, in 2018 (Moretti et al., 2020).

Seismic unrest periods concurrent with deformation are also frequent at calderas. For example, in 2011–2012 Santorini underwent inflation, VT seismicity, and enhanced CO_2 emissions (Parks et al. 2015), with a deformation of 12–14 cm across the archipelago, a deformation source located at 4 km depth, and a seismic moment release of ~10^{15} N·m. In 1997–1998, Long Valley caldera displayed 10 cm of uplift and over 12,000 VT earthquakes with a total moment of ~10^{17} N·m (Hill, 2006). For a comprehensive review of recent periods of unrest at calderas, see Acocella et al., 2015.

In all these cases, the seismic swarms were accompanied by other evidences of magma ascent, such as deformation or increased gas emissions, but no volcanic eruption was produced. Seismic swarms that do not culminate in a magmatic eruption are a consequence of stalled intrusions of magma into the mid- or shallow-level crust. Moran et al., 2011 summarized these evidences and defined a "failed eruption" as a process in which magma has intruded to shallow depths, accompanied by anomalous seismicity, deformation, and degassing, but ultimately fails to reach the surface. If we compare the number of seismic swarms (e.g. Benoit and McNutt, 1996) and the number of magmatic eruptions, it appears that the majority of intrusions stall at some depth without erupting (Moran et al., 2011). A variety of reasons can explain the arrest of the intrusion, including magma solidification in slow-ascending dykes, reduction of magma chamber overpressure, physical barriers related to sharp gradients in mechanical properties, and density stratification.

With this definition, the magma intrusion mechanism invoked to explain the origin of the seismic series that occurred at Deception Island in 1992, 1999, and 2015 is precisely the description of a failed eruption.

However, and despite the similarities between the unrest episodes described above, the 1999 and 2015 series show significant differences. This leads us to think that the magma intrusions that originated the seismic activity had somewhat diverse characteristics.

For example, a first observation is that the temporal occurrence of VT events followed different patterns. The 1999 series displayed a regular

behavior with constant earthquake production rates and stable moment release, except for the two felt earthquakes. On the contrary, in 2015 the activity was largely discontinuous, distributed in temporal clusters with relatively long aseismic periods between them. These differences suggest that the 1999 intrusion was a smoother process, with a constant liberation of energy. The 2015 intrusion, on the contrary, was more irregular and episodic. Rather than a continuous injection of magma, we image it as a series of discontinuous, short-lived pulses that extend in time due to an underlying intrusion process.

From a spatial point of view, we find also two different patterns. In 1999 the majority of VT events were located within Port Foster at shallow depths of 0–4 km, and aligned along a WSW-ENE direction that parallels the Bransfield rift. In 2015 the VT events surrounded the volcanic edifice at distances up to 30 km and depths mostly in the range 0–10 km. The locations did not follow any particular trends, and were basically unrelated to regional tectonics.

The differences in the spatial distributions of earthquakes can be explained in terms of the depth of the intrusion. The presence and extent of a magma plumbing system beneath Deception Island has been addressed by a number of geophysical studies, based on observations of seismic attenuation (Vila et al., 1995; Prudencio et al., 2013, 2015), seismic velocities (Zandomeneghi et al., 2009; Ben-Zvi et al., 2009), magnetic and gravity anomalies (Muñoz-Martín et al., 2005; Catalán et al., 2013, 2014) and resistivity (Pedrera et al., 2012). These studies point to the presence of an anomalous volume beneath the Deception Island caldera, located at depths below 2 km, with a lateral extent of at least the size of the inner bay, and characterized by distinct properties compared to the surrounding crust (low seismic velocity, high attenuation, low resistivity, etc). This volume has been interpreted as a magma accumulation zone with an estimated melt volume of up to 20 km^3 (Ben-Zvi et al., 2009), although other estimates are much larger (e.g. Pedrera et al., 2012). Given the variability in the petrology and geochemistry of volcanic products related to recent eruptions, with magmas ranging from basaltic to rhyolitic, it is unlikely that this anomalous volume is made of a single, extensive magma chamber (Martí et al., 2013). Instead, we image the plumbing system as composed of batches of magma that accumulate at different levels and are connected by a network of sills and dykes, and may include a significant portion of cooling, non-eruptible magma (Geyer et al., 2019; Álvarez-Valero et al., 2020). Based on the interpretation of petrological and geochemical data, Geyer et al., 2019 proposed the existence of several shallow reservoirs at depths of 2–10 km, which would be responsible for the recent eruptions of Deception Island. These reservoirs are fed by magmas raised from the mantle or from an accumulation zone located at the crust-mantle boundary (15–20 km depth).

Fig. 8 shows a conceptual sketch of the plumbing system of Deception Island volcano. The intrusion of magma into a shallow reservoir (A) would produce stress changes in a small volume concentrated between the reservoir and the surface. Consequently, most earthquakes would be produced at shallow depths beneath the caldera, along pre-existing fractures or weak zones. In particular, the WSW-ENE fault system across the northern part of the Deception Island caldera from Fumarole Bay to Pendulum Cove (e.g. Martí et al., 2013), would be an obvious seismogenic zone. The intrusion of magma into a deeper reservoir (B) would have a more distributed effect, producing stress changes in the whole volcanic edifice. Earthquakes could occur in a larger volume, including the flanks of the volcanic edifice, and extending to larger depths. These are precisely the spatial patterns of the 1999 and 2015 seismic series. Therefore, we propose that the 1999 series was consequence of a shallow intrusion reaching a depth around 4 km, while the 2015 series was produced by a deeper intrusion, around 10 km, as suggested by the lower boundary of the earthquake distributions.

Another evidence pointing to a deep intrusion in 2015 is the occurrence of the Livingston series three months before the start of the Deception VT series. Almendros et al., 2018 propose two possibilities to explain the relationship between these series of earthquakes. First, the Livingston series could have induced dynamic stress changes at Deception Island, triggering the intrusion that in turn generated the VT activity. However, given the small magnitudes of the earthquakes ($M < 4.6$), large distances (~35 km), and long delay between the series (~months), this possibility is unlikely. Instead, we favor the second model, where a deep intrusion at Deception Island may have triggered both the Livingston series and the Deception Island VT activity. The occurrence of earthquake series relatively far from the volcanic centers in advance to any VT activity within the volcanic edifice itself is a common phenomenon observed at several volcanoes, and is referred to as distal VT earthquakes (White and McCausland, 2016). Precursory distal VT seismicity may reflect magma-induced fluid-pressure pulses that intersect critically-stressed faults (Coulon et al., 2017; White and McCausland, 2019). The reason for these distal earthquakes is that pressure perturbations through crustal fluids propagate easier in horizontal direction, parallel to the dominant layering, than in vertical direction. If these perturbations reach a weak zone in the distant flanks of the volcano, they may promote series of earthquakes that usually occur before the perturbations reach the summit areas and any volcanic activity is observed. This is represented in Fig. 8 by the cluster of hypocenters located far away from the volcano. A necessary condition is that the originating intrusion must be deep enough; otherwise, its effects would be immediate in the volcanic center itself, and horizontally limited to the volcanic edifice. In the 1999 series, there were no previous distal earthquakes,

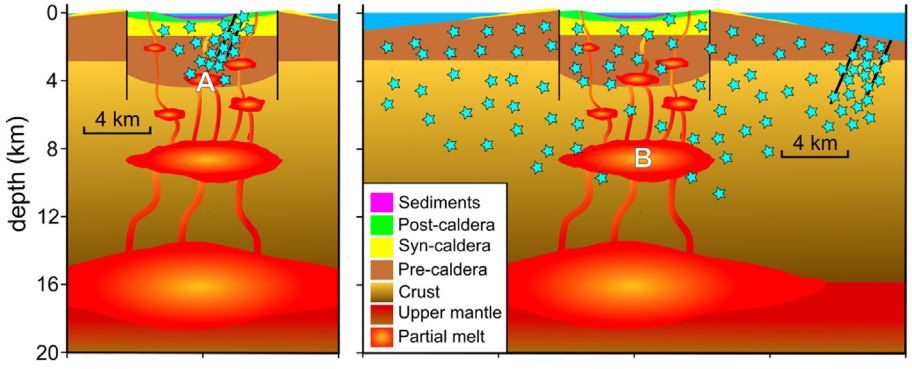

Fig. 8. Sketch of the magma plumbing system and shallow structure of Deception Island volcano based on the model of Geyer et al., 2019. Cyan stars indicate the spatial distribution of VT earthquakes. For a shallow intrusion (left), magma reaches a shallow accumulation zone (A) and the earthquakes cluster at shallow depths beneath Deception Island. For a deep intrusion (right), magma accumulates at some depth (B) and the hypocenters are deeper and spread over a wider zone. Thick black lines indicate brittle regions where the perturbations caused by the intrusion may trigger clusters of VT earthquakes.

which supports the conclusion that the 1999 intrusion was much shallower than the 2015 intrusion.

Additionally, Rosado et al., 2019 provides the parameters of the Mogi sources that best fit the inflation processes accompanying the seismic series. The estimated depths are 3.8 km for 1999 and 6.1 km for 2015. This difference in the Mogi source depth supports our interpretation that the 1999 intrusion was shallower than the 2015 intrusion.

Earthquake magnitudes were generally larger in 2015 than in 1999, even if the maximum magnitudes of the series were the same. The average seismic moment release rate in 2015 is four times larger than the 1999 value, which implies that more seismic energy was involved in the 2015 process. The cumulative seismic moments of the 1999 and 2015 series were $1.6 \cdot 10^{14}$ N·m and $1.8 \cdot 10^{15}$ N·m, respectively, a difference of one order of magnitude. However, we consider that the Livingston series was distal VT seismicity related directly to the failed eruption process. Therefore, it should be included as part of the process, and the total seismic moment rises to $7.8 \cdot 10^{16}$ N·m (Almendros et al., 2018), almost 500 times larger than in 1999.

White and McCausland, 2016 studied the relationship between the volume of the intrusion and the total seismic moment of the precursory distal VT seismicity, for cases in which this volume could be obtained independently of the seismic data. They found that the larger the intruded volume, the larger the cumulative seismic moment, and proposed a formula to estimate the volume of the intrusion from the total seismic moment. An updated calculation of their formula yields the expression $\log_{10}(V) = 0.783 \cdot \log_{10}(M_0) - 6.56$ (W. McCausland, personal communication), where V is the volume of the intrusion in m^3 and M_0 is the total seismic moment in N·m. Using this approach, we estimate that in 1999 the amount of magma intruded was $3.7 \cdot 10^4$ m^3. In 2015, considering the whole process and including the distal VT seismicity, the volume change was $4.6 \cdot 10^6$ m^3, in the range of a VEI 2 eruption. This result is consistent with the volume change of $9.7 \cdot 10^6$ m^3 obtained from GPS observations in 2014 and 2015 (Rosado et al., 2019).

Although the reported durations of the 1999 and 2015 seismic series are comparable, other evidences indicate that the effects of the 2015 failed eruption lasted much longer than the 1999 intrusion. Ibáñez et al. 2003b recorded the 1999 series during 1.5 months, until February 1999 when the survey ended and the Gabriel de Castilla base closed for the winter. Data from a seismometer left at the island demonstrated that the level of seismicity was still high when the instrument failed in early April 1999. However, by the start of the next survey (December 1999) the seismicity was back to normal (Ibáñez et al., 2003b; Berrocoso et al., 2006). Therefore, with no precursory changes in the volcanic system, the duration of the 1999 failed eruption process can be narrowed down to 4–11 months. In the case of the 2015 series, the VT seismicity at Deception Island volcano had a duration of 5 months, as reported by Almendros et al., 2018. However, the results of seismic monitoring surveys carried out during the austral summer months after 2015 indicate that the VT activity at Deception Island was anomalously high at least for 3 years (Fig. 2). Similarly, the level of LP seismicity increased drastically between 2014 and 2018, reaching a maximum of activity during the 2015–2016 seismic survey.

Moreover, the Livingston series, considered here as distal VT seismicity, had a reported duration of 8 months from September 2014 to May 2015 (Almendros et al., 2018). However, several earthquakes were detected in the same epicentral area many months later. Dimitrova et al., 2017 analyzed earthquakes recorded during December 2015–February 2016 by a seismometer located at the Bulgarian base in Livingston Island. They documented a cluster of ~25 small earthquakes ($M < 2$) that occurred SE of Livingston, precisely in the same area than the 2014–2015 Livingston series.

Therefore, the events related to the 2015 failed eruption seem to extend in time much longer than in 1999. The deep intrusion could have started in early 2014, or even earlier as suggested by deformation data (Rosado et al., 2019; Berrocoso et al., 2018). The intrusion produced a perturbation that propagated through crustal fluids. The perturbation reached a seismogenic zone SE of Livingston by September 2014, when the Livingston series started (Almendros et al., 2018). This area is located NE of Deception Island along the Bransfield rift, which might explain the preferential propagation of the perturbation in that direction. At that time, no significant VT seismicity was reported yet at Deception Island. In December 2014 we started to detect VT earthquakes in the Sail Rock area, located ~20 km SW of Deception Island (Almendros et al., 2018), which is also located along the rift, but in the opposite direction. Hence, this cluster could be regarded as distal VT seismicity as well. Finally, by February 2015 there was a generalized activation of faults across the volcanic edifice. The level of seismicity at Deception Island remained high for a few years, and the volcano did not return to the background state perhaps until 2018.

5. Conclusions

We have compared the three seismic crises recorded at Deception Island volcano in the last decades. Although they share some characteristics such as the earthquake production rates and maximum magnitudes, they also display significant differences. The 1999 series comprised mostly small-magnitude earthquakes, produced regularly during 1.5 months, and located at shallow depths (<4 km) within the caldera, mostly along a WSW-ENE trend that parallels the Bransfield rift. The 2015 series included earthquakes with larger magnitudes, occurring during 5 months in temporal clusters separated by aseismic periods. They were located at deeper levels (<10 km) with epicenters distributed all around Deception Island, at distances up to 30 km. Additionally, distal VT seismicity was reported SE of Livingston (and also SW of Deception Island) months before the 2015 series onset. The 1992 series apparently shares the tight spatial distribution of the 1999 series, and the irregular temporal pattern of the 2015 series. Unfortunately, in this case the lack of a quantitative earthquake catalog prevents any further conclusions.

The mechanism invoked to explain the origin of these three seismic crises is a magmatic intrusion that stalled before reaching the surface, and therefore did not produce an eruption (Ortiz et al. 1997; Ibáñez et al., 2003b; Almendros et al., 2018). Similar processes have been observed at different volcanoes, and their interpretation has given birth to the concept of "failed eruption" (Moran et al., 2011).

In any case, given the differences observed in the behavior of the series, we conclude that they could not be originated by identical processes. The 1999 series was produced by a shallow intrusion affecting the shallowmost part of the volcanic edifice, while the 2015 series was consequence of a deep intrusion that modified the stress field of the whole volcano. Estimates of the intrusion volumes based on the total seismic moment (White and McCausland, 2016) yield ~$4 \cdot 10^4$ m^3 for 1999 and ~ $5 \cdot 10^6$ m^3 for 2015, a difference of two orders of magnitude. Additionally, the durations of the unrest periods were very different as well. Considering the seismicity and deformation reported at Deception Island at these periods, we estimate that the effects of the 1999 intrusion lasted for 4–11 months, while the effects of the 2015 intrusion were more persistent and lasted for at least a few years.

With these considerations, we envisage the 2015 series as the result of a deep, large-volume, long-lasting magma intrusion, while the 1999 series was produced by a shallow, small-volume intrusion in a shorter time span. Because of this, Deception Island might have been closer to an eruption in 1999. Nevertheless, the 2015 failed eruption has contributed to raise a significant volume of fresh magma to shallower levels, which may have increased the amount of eruptible magma in the shallow plumbing system. Although historical eruptions have been generally small, larger eruptions are possible as well (Geyer et al., 2019). Therefore, we must be aware of the possibilities that this situation opens for the future. Continuing research and monitoring are crucial to improve the hazards assessment at Deception Island volcano.

Data

Earthquake data are available through Ortiz et al., 1997, Ibáñez et al., 2003b, and Almendros et al., 2018. The VT earthquake catalogs used in this paper to compare the 1999 and 2015 seismic series can be accessed through the Zenodo repository (https://doi.org/10.5281/zenodo.4634904).

Declaration of Competing Interest

The authors declare that they have no known competing financial interests or personal relationships that could have appeared to influence the work reported in this paper.

Acknowledgements

The work of AMV was funded by a Grant for Young Researchers (ref. 2018-6032) under the Youth Employment Program of the Junta de Andalucía, Spain. Additional support comes from project BRAVOSEIS funded by the Spanish Ministry of Science (MINECO) under grant CTM2016-77315-R. Funding for the open access charges comes from Univeristy of Granada / CBUA.

References

Acocella, V., Di Lorenzo, R., Newhall, C., Scandone, R., 2015. An overview of recent (1988 to 2014) caldera unrest: Knowledge and perspectives. Rev. Geophys. 53, 896–955. https://doi.org/10.1002/2015RG000492.

Almendros, J., Ibáñez, J.M., Alguacil, G., Del Pezzo, E., Ortiz, R., 1997. Array tracking of the volcanic tremor source at Deception Island, Antarctica. Geophys. Res. Lett. 24 (23), 3069–3072. https://doi.org/10.1029/97GL03096.

Almendros, J., Ibáñez, J.M., Alguacil, G., Del Pezzo, E., 1999. Array analysis using circular-wave-front geometry: an application to locate the nearby seismo-volcanic source. Geophys. J. Int. 136 (1), 159–170. https://doi.org/10.1046/j.1365-246X.1999.00699.x.

Almendros, J., Carmona, E., Ibáñez, J.M., 2004. Precise determination of the relative wave propagation parameters of similar events using a small-aperture seismic array. J. Geophys. Res. 109, B11308. https://doi.org/10.1029/2003JB002930.

Almendros, J., Ibáñez, J.M., Carmona, E., Zandomeneghi, D., 2007. Array analyses of volcanic earthquakes and tremor recorded at Las Cañadas caldera (Tenerife Island, Spain) during the 2004 seismic activation of Teide volcano. J. Volcanol. Geotherm. Res. 160 (3–4), 285–299. https://doi.org/10.1016/j.jvolgeores.2006.10.002.

Almendros, J., Carmona, E., Jiménez-Morales, V., Díaz-Moreno, A., Lorenzo, F., Berrocoso, M., et al., 2015. Deception Island (Antarctica): Sustained deformation and large increase in seismic activity during 2014-2015. In: Venzke, E. (Ed.), Bulletin of the Global Volcanism Network 40. Smithsonian Institution.

Almendros, J., Carmona, E., Jiménez-Morales, V., Díaz-Moreno, A., Lorenzo, F., 2018. Volcano-tectonic activity at Deception Island volcano following a seismic swarm in the Bransfield Rift (2014-2015). Geophys. Res. Lett. 45, 4788–4798. https://doi.org/10.1029/2018GL077490.

Almendros, J., Wilcock, W., Soule, D., Teixidó, T., Vizcaíno, L., Ardanaz, O., Granja-Bruña, J.L., Martín-Jiménez, D., Yuan, X., Heit, B., Schmidt-Aursch, M.C., Geissler, W., Dziak, R., Carrión, F., Ontiveros, A., Abella, R., Carmona, E., Agüí-Fernández, J.F., Sánchez, N., Serrano, I., Davoli, R., Krauss, Z., Kidiwela, M., Schmahl, L., 2020. BRAVOSEIS: Geophysical investigation of rifting and volcanism in the Bransfield Strait, Antarctica. J. S. Am. Earth Sci. 104, 102834. https://doi.org/10.1016/j.jsames.2020.102834.

Álvarez-Valero, A.M., Gisbert, G., Aulinas, M., Geyer, A., Kereszturi, G., Polo-Sánchez, A., Núñez-Guerrero, E., Sumino, H., Borrajo, J., 2020. δD and $\delta^{18}O$ variations of the magmatic system beneath Deception Island volcano (Antarctica): implications for magma ascent and eruption forecasting. Chem. Geol. 542, 119595. https://doi.org/10.1016/j.chemgeo.2020.119595.

Antoniades, D., Giralt, S., Geyer, A., Álvarez-Valero, A.M., Pla-Rabes, S., Granados, I., Liu, E.J., Toro, M., Smellie, J.L., Oliva, M., 2018. The timing and widespread effects of the largest Holocene volcanic eruption in Antarctica. Sci. Rep. 8, 17279. https://doi.org/10.1038/s41598-018-35460-x.

Baker, P.E., McReath, I., Harvey, M.R., Roobol, M.J., Davies, T.G., 1975. The Geology of the South Shetland Islands: Volcanic evolution of Deception Island. Br. Antarct. Surv. Scientific Reports 78, 81.

Barclay, A.H., Wilcock, W., Ibáñez, J.M., 2009. Bathymetric constraints on the tectonic and volcanic evolution of Deception Island Volcano, South Shetland Islands. Antarct. Sci. 21 (2), 153–167. https://doi.org/10.1017/S0954102008001673.

Bartolini, S., Geyer, A., Martí, J., Pedrazzi, D., Aguirre-Díaz, G., 2014. Volcanic hazard on Deception Island (South Shetland Islands, Antarctica). J. Volcanol. Geotherm. Res. 285, 150–168. https://doi.org/10.1016/j.jvolgeores.2014.08.009.

Benítez, M.C., Ramírez, J., Segura, J.C., Ibáñez, J.M., Almendros, J., García-Yeguas, A., Cortés, G., 2007. Continuous HMM-based seismic-event classification at Deception Island, Antarctica. IEEE Trans. Geosci. Remote Sens. 45 (1), 138–146. https://doi.org/10.1109/TGRS.2006.882264.

Benoit, J.P., McNutt, S.R., 1996. Global volcanic earthquake swarm database and preliminary analysis of volcanic earthquakes swarm duration. Ann. Geofis. 39, 221–229.

Ben-Zvi, T., Wilcock, W., Barclay, A., Zandomeneghi, D., Ibáñez, J.M., Almendros, J., 2009. The P-wave velocity structure of Deception Island, Antarctica, from two-dimensional seismic tomography. J. Volcanol. Geotherm. Res. 180 (1), 67–80. https://doi.org/10.1016/j.jvolgeores.2008.11.020.

Berrocoso, M., García-García, A., Martín-Dávila, J., Catalán-Morollón, M., Astiz, M., Ramírez, M.E., Torrecillas, C., Enríquez de Salamanca, J.M., Futterer, D.K., 2006. Geodynamical Studies on Deception Island: DECVOL and GEODEC Projects. In: Damaske, D., Kleinschmidt, G., Miller, H., Tessensohn, F. (Eds.), Antarctica. Springer, pp. 283–287 https://doi.org/10.1007/3-540-32934-X_35.

Berrocoso, M., Prates, G., Fernández-Ros, A., Peci, L.M., de Gil, A., Rosado, B., Páez, R., Jigena, B., 2018. Caldera unrest detected with seawater temperature anomalies at Deception Island, Antarctic Peninsula. Bull. Volcanol. 80 (4), 41. https://doi.org/10.1007/s00445-018-1216-2.

Carmona, E., Almendros, J., Peña, J.A., Ibáñez, J.M., 2010. Characterization of fracture systems using precise array locations of earthquake multiplets: an example at Deception Island volcano, Antarctica. J. Geophys. Res. 115, B06309. https://doi.org/10.1029/2009JB006865.

Carmona, E., Almendros, J., Martín, R., Serrano, I., Stich, D., Ibáñez, J.M., 2012. Results of seismic monitoring surveys of Deception Island volcano, Antarctica, from 1999-2011. Antarct. Sci. 24, 485–499. https://doi.org/10.1017/S0954102012000314.

Carmona, E., Almendros, J., Martín, R., Cortés, G., Alguacil, G., Moreno, J., et al., 2014. Advances in seismic monitoring at Deception Island volcano (Antarctica) since the International Polar Year. Ann. Geophys. 57 (3), SS0321. https://doi.org/10.4401/ag-6378.

Casadevall, T.J., Greenland, P.L., 1981. The chemistry of gases emanating from Mount St. Helens, May-September 1980. In: Lipman, P.W., Mullineaux, D.R. (Eds.), The 1980 Eruptions of Mount St. Helens, Washington, U.S. Geological Survey, Prof. Paper. 1250, pp. 221–226.

Caselli, A.T., Santos-Afonso, M., Agusto, M.R., 2004. Gases fumarólicos de la isla Decepción (Shetlands del Sur, Antártida): variaciones químicas y depósitos vinculados a la crisis sísmica de 1999. Rev. Asoc. Geol. Argent. 59, 291–302.

Caselli, A.T., Badi, G., Bonatto, A.L., Bengoa, C.L., Agusto, M.R., Bidone, A., Ibáñez, J.M., 2007. Actividad sísmica y composición química fumarólica anómala debido a posible efecto sello en el sistema volcánico, Isla Decepción (Antártida). Rev. Asoc. Geol. Argent. 62, 545–552.

Catalán, M., Galindo-Zaldívar, J., Martín-Dávila, J., Martos, Y.M., Maldonado, A., Gamboa, L., Schreider, A.A., 2013. Initial stages of oceanic spreading in the Bransfield Rift from magnetic and gravity data analysis. Tectonophysics 585, 102–112. https://doi.org/10.1016/j.tecto.2012.09.016.

Catalán, M., Martos, Y.M., Galindo-Zaldívar, J., Funaki, M., 2014. Monitoring the evolution of Deception Island volcano from magnetic anomaly data (South Shetland Islands, Antarctica). Global Planet. Change 123, Part B, 199–212 https://doi.org/10.1016/j.gloplacha.2014.07.018.

Cembrano, J., Lara, L., 2009. The link between volcanism and tectonics in the southern volcanic zone of the Chilean Andes: a review. Tectonophysics 471, 96–113. https://doi.org/10.1016/j.tecto.2009.02.038.

Chouet, B., 2003. Volcano Seismology. Pure Appl. Geophys. 160, 739–788. https://doi.org/10.1007/PL00012556.

Christeson, G.L., Barker, D.H.N., Austin, J.A., Dalziel, I.W.D., 2003. Deep crustal structure of Bransfield Strait: Initiation of a back arc basin by rift reactivation and propagation. J. Geophys. Res. 108 (B10), 2492. https://doi.org/10.1029/2003JB002468.

Coulon, C., Hsieh, P., White, R., Lowenstern, J., Ingebritsen, S., 2017. Causes of distal volcano-tectonic seismicity inferred from hydrothermal modeling. J. Volcanol. Geotherm. Res. 345, 98–108. https://doi.org/10.1016/j.jvolgeores.2017.07.011.

Cusano, P., Petrosino, S., Saccorotti, G., 2008. Hydrothermal origin for sustained Long-Period (LP) activity at Campi Flegrei Volcanic complex, Italy. J. Volcan. Geotherm. Res. 177, 1035–1044. https://doi.org/10.1016/j.jvolgeores.2008.07.019.

Del Pezzo, E., La Rocca, M., Ibáñez, J.M., 1997. Observations of high-frequency scattered waves using dense arrays at Teide volcano. Bull. Seismol. Soc. Am. 87, 1637–1647.

Dimitrova, L., Georgieva, G., Raykova, R., Dimitrov, D., Gurev, V., Solakov, D., Georgiev, I., Raykova, P., Protopopova, V., Aleksandrova, I., Popova, M., 2017. Exploring Seismicity of Livingston Island (Antarctica) and Surroundings using Records of Bulgarian Broadband Seismological Station LIVV during the Austral Summer 2015-2016. Comptes Rendus Bulgarian Acad. Sci. 70, 1709–1718.

Domínguez-Cerdeña, I., Del Fresno, C., Rivera, L., 2011. New insight on the increasing seismicity during Tenerife's 2004 volcanic reactivation. J. Volcanol. Geotherm. Res. 206 (1–2), 15–29. https://doi.org/10.1016/j.jvolgeores.2011.06.005.

Galindo-Zaldívar, J., Gamboa, L., Maldonado, A., Nakao, S., Bochu, Y., 2004. Tectonic development of the Bransfield Basin and its prolongation to the South Scotia Ridge, northern Antarctic Peninsula. Mar. Geol. 206 (1–4), 267–282. https://doi.org/10.1016/j.margeo.2004.02.007.

García, A., Blanco, I., Torta, J.M., Astiz, M., Ibáñez, J.M., Ortiz, R., 1997. A search for the volcano-magnetic signal at Deception volcano (South Shetland Islands, Antarctica). Ann. Geophys. 40, 319–327. https://doi.org/10.4401/ag-3914.

García-Yeguas, A., Almendros, J., Abella, R., Ibáñez, J.M., 2011. Quantitative analysis of seismic wave propagation anomalies in azimuth and apparent slowness at Deception Island volcano (Antarctica) using seismic arrays. Geophys. J. Int. 184, 801–815. https://doi.org/10.1111/j.1365-246X.2010.04864.x.

Gardine, M., West, M.E., Cox, T., 2011. Dike emplacement near Parícutin volcano, Mexico in 2006. Bull. Volcanol. 73, 123–132. https://doi.org/10.1007/s00445-010-0437-9.

Geyer, A., Martí, J., 2008. The new worldwide collapse caldera database (CCDB): a tool for studying and understanding caldera processes. J. Volcanol. Geotherm. Res. 175, 334–354. https://doi.org/10.1016/j.jvolgeores.2008.03.017.

Geyer, A., Álvarez-Valero, A.M., Gisbert, G., et al., 2019. Deciphering the evolution of Deception Island's magmatic system. Sci. Rep. 9, 373. https://doi.org/10.1038/s41598-018-36188-4.

Geyer, A., Pedrazzi, D., Almendros, J., Berrocoso, M., López-Martínez, J., Maestro, A., Carmona, E., Álvarez-Valero, A.M., De Gil, A., 2021. Deception Island. In: Smellie, J., Panter, K.S., Geyer, A. (Eds.), Volcanism in Antarctica: 200 Million Years of Subduction, Rifting and Continental Break-Up. Geological Society of London, Memoirs, p. 55 https://doi.org/10.1144/M55-2018-56.

González-Ferrán, O., 1985. Volcanic and tectonic evolution of the northern Antarctic Peninsula - late Cenozoic to recent. Tectonophysics 114, 389–409. https://doi.org/10.1016/0040-1951(85)90023-X.

Gordon, A.L., Nowlin, W.D., 1978. Basin waters of Bransfield Strait. J. Phys. Oceanogr. 8, 258–264. https://doi.org/10.1175/1520-0485(1978)008<0258:TBWOTB>2.0.CO;2.

Gudmundsson, A., 2020. Volcanotectonics. Cambridge University Press, p. 586 https://doi.org/10.1017/9781139176217.

Havskov, J., Peña, J.A., Ibáñez, J.M., Ottemoller, L., Martínez-Arévalo, C., 2003. Magnitude scales for very local earthquakes. Application for Deception Island Volcano (Antarctica). J. Volcanol. Geotherm. Res. 128, 115–133. https://doi.org/10.1016/S0377-0273(03)00250-6.

Heinicke, J., Fischer, T., Gaupp, R., Gotze, J., Koch, U., Konietzky, H., Stanek, K.-P., 2009. Hydrothermal alteration as a trigger mechanism for earthquake swarms: the Vogtland/NW Bohemia region as a case study. Geophys. J. Int. 178, 1–13. https://doi.org/10.1111/j.1365-246X.2009.04138.x.

Hill, D.P., 2006. Unrest in Long Valley Caldera, California, 1978–2004. Geol. Soc. London Spec. Publ. 269 (1), 1–24. https://doi.org/10.1144/GSL.SP.2006.269.01.02.

Ibáñez, J.M., Morales, J., Alguacil, G., Almendros, J., Ortiz, R., Del Pezzo, E., 1997. Intermediate-focus earthquakes under South Shetland Islands, Antarctica. Geophys. Res. Lett. 24 (5), 531–534. https://doi.org/10.1029/97GL00314.

Ibáñez, J.M., Del Pezzo, E., Almendros, J., La Rocca, M., Alguacil, G., Ortiz, R., García, A., 2000. Seismovolcanic signals at Deception Island volcano, Antarctica: Wave field analysis and source modeling. J. Geophys. Res. 105 (B6), 13905–13931. https://doi.org/10.1029/2000JB900013.

Ibáñez, J.M., Almendros, J., Carmona, E., Martínez-Arévalo, C., Abril, M., 2003a. The recent seismo-volcanic activity at Deception Island volcano. Deep-Sea Res. II 50 (10−11), 1611–1629. https://doi.org/10.1016/S0967-0645(03)00082-1.

Ibáñez, J.M., Carmona, E., Almendros, J., Saccorotti, G., Del Pezzo, E., Abril, M., Ortiz, R., 2003b. The 1998-1999 seismic series at Deception Island volcano, Antarctica. J. Volcanol. Geotherm. Res. 128 (1–3), 65–88. https://doi.org/10.1016/S0377-0273(03)00247-6.

Ibáñez, J.M., Díaz-Moreno, A., Prudencio, J., Zandomeneghi, D., Wilcock, W., Barclay, A., et al., 2017. Database of multi-parametric geophysical data from the Tomodec experiment on Deception Island, Antarctica. Scientific Data 4, 170128. https://doi.org/10.1038/sdata.2017.128.

Jay, J.A., Delgado, F.J., Torres, J.L., Pritchard, M.E., Macedo, O., Aguilar, V., 2015. Deformation and seismicity near Sabancaya volcano, southern Peru, from 2002 to 2015. Geophys. Res. Lett. 42, 2780–2788. https://doi.org/10.1002/2015GL063589.

Jiménez-Morales, V., Almendros, J., Carmona, E., 2017. Detection of long-duration tremors at Deception Island volcano, Antarctica. J. Volcanol. Geotherm. Res. 347, 234–249. https://doi.org/10.1016/j.jvolgeores.2017. 09.016.

Jiménez-Morales, V., Almendros, J., Carmona, E., 2021. Analysis of the seismic activity preceding the 2015 seismic crisis at Deception Island volcano, Antarctica, usign continuous data from a permanent broadband seismic station (2008-2015) (submitted).

Jolly, A.D., Lokmer, I., Thun, J., Salichon, J., Fry, B., Chardot, L., 2017. Insights into fluid transport mechanisms at White Island from analysis of coupled very long-period (VLP), long-period (LP) and high-frequency (HF) earthquakes. J. Volcanol. Geotherm. Res. 343, 75–94. https://doi.org/10.1016/j.jvolgeores.2017.06.006.

Koulakov, I., El Khrepy, S., Al-Arifi, N., Kuznetsov, P., Kasatkina, E., 2015. Structural cause of a missed eruption in the Harrat Lunayyir basaltic field (Saudi Arabia) in 2009. Geology 43, 395–398. https://doi.org/10.1130/G36271.1.

Lu, Z., Wicks, C., Power, J.A., Dzurisin, D., 2000. Ground deformation associated with the March 1996 earthquake swarm at Akutan volcano, Alaska, revealed by satellite radar interferometry. J. Geophys. Res. 105 (B9), 21483–21495. https://doi.org/10.1029/2000JB900200.

Luzón, F., Almendros, J., García-Jerez, A., 2011. Shallow structure of Deception Island, Antarctica, from correlations of ambient seismic noise on a set of dense seismic arrays. Geophys. J. Int. 185, 737–748. https://doi.org/10.1111/j.1365-246X.2011.04962.x.

Maestro, A., Somoza, L., Rey, J., Martínez-Frías, J., López-Martínez, J., 2007. Active tectonics, fault patterns, and stress field of Deception Island: a response to oblique convergence between the Pacific and Antarctic plates. J. S. Am. Earth Sci. 23 (2–3), 256–268. https://doi.org/10.1016/j.jsames.2006.09.023.

Maldonado, A., Dalziel, I.W.D., Leat, P.T., 2015. The global relevance of the Scotia Arc: an introduction. Glob. Planet. Chang. 125, A1–A8. https://doi.org/10.1016/j.gloplacha.2014.06.011.

Martí, J., Vila, J., Rey, J., 1996. Deception Island (Bransfield Strait, Antarctica): an example of a volcanic caldera developed by extensional tectonics. Geol. Soc. Lond. Spec. Publ. 110 (1), 253–265. https://doi.org/10.1144/GSL.SP.1996.110.01.20.

Martí, J., Geyer, A., Aguirre-Diaz, G., 2013. Origin and evolution of the Deception Island caldera (South Shetland Islands, Antarctica). Bull. Volcanol. 75 (1–18). https://doi.org/10.1007/s00445-013-0732-3.

McNutt, S.R., 2005. Volcanic Seismology. Annu. Rev. Earth Planet. Sci. 32, 461–491. https://doi.org/10.1146/annurev.earth.33.092203.122459.

Mesimeri, M., Pankow, K.L., Baker, B., Hale, J.M., 2021. Episodic earthquake swarms in the Mineral Mountains, Utah driven by the Roosevelt hydrothermal system. J. Geophys. Res. Solid Earth 126, e2021JB021659. https://doi.org/10.1029/2021JB021659.

Moran, S.C., Newhall, C., Roman, D.C., 2011. Failed magmatic eruptions: late-stage cessation of magma ascent. Bull. Volcanol. 73, 115–122. https://doi.org/10.1007/s00445-010-0444-x.

Moretti, R., Komorowski, J.-C., Ucciani, G., Moune, S., Jessop, D., de Chabalier, J.-B., Beauducel, F., Bonifacie, M., Burtin, A., Vallée, M., Deroussi, S., Robert, V., Gibert, D., Didier, T., Kitou, T., Feuillet, N., Allard, P., Tamburello, G., Shreve, T., Saurel, J.-M., Lemarchand, A., Rosas-Carbajal, M., Agrinier, P., Le Friant, A., Chaussidon, M., 2020. The 2018 unrest phase at La Soufriere of Guadeloupe (French West Indies) andesitic volcano: Scrutiny of a failed but prodromal phreatic eruption. J. Volcanol. Geotherm. Res. 393, 106769. https://doi.org/10.1016/j.jvolgeores.2020.106769.

Muñoz-Martín, A., Catalán, M., Martín-Dávila, J., Carbó, A., 2005. Upper crustal structure of Deception Island area (Bransfield Strait, Antarctica) from gravity and magnetic modelling. Antarct. Sci. 17, 213–224. https://doi.org/10.1017/S0954102005002622.

Nakano, M., Kumagai, H., 2005. Response of a hydrothermal system to magmatic heat inferred from temporal variations in the complex frequencies of long-period events at Kusatsu-Shirane volcano, Japan. J. Volcanol. Geotherm. Res. 147, 233–244. https://doi.org/10.1016/j.jvolveores.2005.04.003.

Nishimura, T., Ueki, S., 2011. Seismicity and magma supply rate of the 1998 failed eruption at Iwate volcano, Japan. Bull. Volcanol. 73, 133–142. https://doi.org/10.1007/s00445-010-0438-8.

Oliva-Urcia, B., Gil-Peña, I., Maestro, A., López-Martínez, J., Galindo-Zaldívar, J., Soto, R., Gil-Imaz, A., Rey, J., Pueyo, O., 2016. Paleomagnetism from Deception Island (south Shetlands archipelago, Antarctica), new insights into the interpretation of the volcanic evolution using a geomagnetic model. Int. J. Earth Sci. (Geol Rundsch) 105, 1353–1370. https://doi.org/10.1007/s00531-015-1254-3.

Ortiz, R., Vila, J., García, A., Camacho, A.G., Díez, J.L., Aparicio, A., Soto, R., Viramonte, J.G., Risso, C., Menegatti, N., Petrinovic, I., 1992a. Geophysical features of Deception Island. In: Yoshida, Y., Kaminuma, K., Shiraishi, K. (Eds.), Recent Progress in Antarctic Earth Science, pp. 443–448.

Ortiz, R., Risso, C., Viramonte, J., 1992b. Deception Island (Antarctica): Increased seismicity, thermal activity, and uplift. In: McClelland, L. (Ed.), Bulletin of the Global Volcanism Network, 17:1. Smithsonian Institution https://doi.org/10.5479/si.GVP.BGVN199201-390030.

Ortiz, R., García, A., Risso, C., Viramonte, J., 1992c. Deception Island (Antarctica): Increased seismicity and thermal activity; uplift. In: McClelland, L. (Ed.), Bulletin of the Global Volcanism Network, 17:4. Smithsonian Institution https://doi.org/10.5479/si.GVP.BGVN199204-390030.

Ortiz, R., García, A., Aparicio, A., Blanco, I., Felpeto, A., Del-Rey, R., et al., 1997. Monitoring of the volcanic activity of Deception Island, South Shetland Islands, Antarctica (1986-1995). In: Ricci, C.A. (Ed.), The Antarctic Region: Geological Evolution and Processes. Terra Antarctica Publication, Siena, Italy, pp. 1071–1076.

Paredes, C., Pérez-López, R., Giner-Robles, J.L., De la Vega, R., García-García, A., Gumiel, P., 2006. Distribución espacial y zonificación tectónica de los morfolineamientos en la Isla Decepción (Shetlands del Sur, Antártida). Geogaceta 39, 75–78.

Parks, M.M., Moore, J.D.P., Papanikolaou, X., Biggs, J., Mather, T.A., Pyle, D.M., Raptakis, C., Paradissis, D., Hooper, A., Parsons, B., Nomikou, P., 2015. From quiescence to unrest: 20 years of satellite geodetic measurements at Santorini volcano. Greece. J. Geophys. Res. Solid Earth 120, 1309–1328. https://doi.org/10.1002/2014JB011540.

Pedrazzi, D., Aguirre-Díaz, G., Bartolini, S., Martí, J., Geyer, A., 2014. The 1970 eruption on Deception Island (Antarctica): eruptive dynamics and implications for volcanic hazards. J. Geol. Soc. 171, 765–778. https://doi.org/10.1144/jgs2014-015.

Pedrazzi, D., Németh, K., Geyer, A., Álvarez-Valero, A.M., Aguirre-Díaz, G., Bartolini, S., 2018. Historic hydrovolcanism at Deception Island (Antarctica): implications for eruption hazards. Bull. Volcanol. 80, 11. https://doi.org/10.1007/s00445-017-1186-9.

Pedrera, A., Ruiz-Constán, A., Heredia, N., Galindo-Zaldívar, J., Bohoyo, F., Marín-Lechado, C., Ruano, P., Somoza, L., 2012. The fracture system and the melt emplacement beneath the Deception Island active volcano, South Shetland Islands, Antarctica. Antarct. Sci. 24, 173–182. https://doi.org/10.1017/S0954102011000794.

Prudencio, J., Ibáñez, J.M., García-Yeguas, A., Del Pezzo, E., Posadas, A.M., 2013. Spatial distribution of intrinsic and scattering seismic attenuation in active volcanic islands, II: Deception Island images. Geophys. J. Int. 195 (3), 1957–1969. https://doi.org/10.1093/gji/ggt360.

Prudencio, J., De Siena, L., Ibáñez, J.M., Del Pezzo, E., García-Yeguas, A., Díaz-Moreno, A., 2015. The 3D attenuation structure of Deception Island (Antarctica). Surv. Geophys. 36 (3), 371–390. https://doi.org/10.1007/s10712-015-9322-6.

Roberts, N.S., Bell, A.F., Main, I.G., 2015. Are volcanic seismic b-values high, and if so when? J. Volcanol. Geotherm. Res. 308, 127–141. https://doi.org/10.1016/j.jvolgeores.2015.10.021.

Roman, D.C., Cashman, K.V., 2006. The origin of volcano-tectonic earthquake swarms. Geology 34, 457–460. https://doi.org/10.1130/G22269.1.

Roman, D.C., Power, J.A., 2011. Mechanism of the 1996-97 non-eruptive volcano-tectonic earthquake swarm at Iliamna Volcano, Alaska. Bull. Volcanol. 73, 143–153. https://doi.org/10.1007/s00445-010-0439-7.

Rosado, B., Fernández-Ros, A., Berrocoso, M., Prates, G., Gárate, J., de Gil, A., Geyer, A., 2019. Volcano-tectonic dynamics of Deception Island (Antarctica): 27 years of GPS observations (1991-2018). J. Volcanol. Geotherm. Res. 381, 57–82. https://doi.org/10.1016/j.jvolgeores.2019.05.009.

Saccorotti, G., Almendros, J., Carmona, E., Ibáñez, J.M., Del Pezzo, E., 2001. Slowness anomalies from two dense seismic arrays at Deception Island, Antarctica. Bull. Seismol. Soc. Am. 91, 561–571. https://doi.org/10.1785/0120000073.

Shepherd, J.B., Tomblin, J.F., Woo, D.A., 1971. Volcano-seismic crisis in Montserrat, West Indies, 1966-67. Bull. Volcanol. 35, 143–163. https://doi.org/10.1007/BF02596813.

Smellie, J.L., 2002. The 1969 subglacial eruption on Deception Island (Antarctica): Events and processes during an eruption beneath a thin glacier and implications for volcanic hazards. In: Smellie, J.L., Chapman, M.G. (Eds.), Volcano-Ice Interaction on Earth and Mars. Geological Society of London Special Publications 202, pp. 59–79 https://doi.org/10.1144/GSL.SP.2002.202.01.04.

Smellie, J.L., López-Martínez, J., Headland, R.K., Hernández-Cifuentes, F., Maestro, A., Millar, I.L., Rey, J., Serrano, E., Somoza, L., Thomson, J.W., 2002. Geology and

Geomorphology of Deception Island. BAS GEOMAP Series, Sheets 6-a and 6-B, 1: 25000, 78 Pp., with Accompanying Maps. British Antarctic Survey, Cambridge.
Vila, J., Martí, J., Ortiz, R., García, A., Correig, A.M., 1992. Volcanic tremors at Deception Island (South Shetland Islands, Antarctica). J. Volcanol. Geotherm. Res. 53, 89–102. https://doi.org/10.1016/0377-0273(92)90076-P.
Vila, J., Correig, A.M., Martí, J., 1995. Attenuation and source parameters at Deception Island (South Shetland Islands, Antarctica), Pure Appl. Geophys. 136, 229–250. https://doi.org/10.1007/BF00878633.
White, R., McCausland, W., 2016. Volcano-tectonic earthquakes: a new tool for estimating intrusive volumes and forecasting eruptions. J. Volcanol. Geotherm. Res. 309, 139–155. https://doi.org/10.1016/j. jvolgeores.2015.10.020.
White, R., McCausland, W., 2019. A process-based model of pre-eruption seismicity patterns and its use for eruption forecasting at dormant stratovolcanoes. J. Volcanol. Geotherm. Res. 382, 267–297. https://doi.org/10.1016/j. jvolgeores.2019.03.004.
Zandomeneghi, D., Barclay, A., Almendros, J., Ibáñez, J.M., Wilcock, W.S.D., Ben-Zvi, T., 2009. Crustal structure of Deception Island volcano from P wave seismic tomography: Tectonic and volcanic implications. J. Geophys. Res. 114, B06310. https://doi.org/10.1029/2008JB006119.
Zobin, V.M., 2017. Introduction to Volcanic Seismology (3rd Edition). Elsevier, p. 582 https://doi.org/10.1016/C2015-0-00304-5.